

# SCIENTIFIC REPORTS

OPEN

## The Henna pigment Lawsone activates the Aryl Hydrocarbon Receptor and impacts skin homeostasis

Laura Lozza<sup>1</sup>, Pedro Moura-Alves<sup>1,2</sup>, Teresa Domaszewska<sup>1</sup>, Carolina Lage Crespo<sup>3</sup>, Ioana Streata<sup>4</sup>, Annika Kreuchwig<sup>5</sup>, Andreas Puyskens<sup>1</sup>, Marina Bechtle<sup>1</sup>, Marion Klemm<sup>1</sup>, Ulrike Zedler<sup>1</sup>, Bogdan Silviu Ungureanu<sup>6</sup>, Ute Gühlich-Bornhof<sup>1</sup>, Anne-Britta Koehler<sup>1</sup>, Manuela Stäber<sup>1</sup>, Hans-Joachim Mollenkopf<sup>7</sup>, Robert Hurwitz<sup>8</sup>, Jens Furkert<sup>5</sup>, Gerd Krause<sup>5</sup>, January Weiner 3rd<sup>1</sup>, António Jacinto<sup>3</sup>, Ioana Mihai<sup>4</sup>, Maria Leite-de-Moraes<sup>9</sup>, Frank Siebenhaar<sup>10</sup>, Marcus Maurer<sup>10</sup> & Stefan H. E. Kaufmann<sup>1,11</sup>

As a first host barrier, the skin is constantly exposed to environmental insults that perturb its integrity. Tight regulation of skin homeostasis is largely controlled by the aryl hydrocarbon receptor (AhR). Here, we demonstrate that Henna and its major pigment, the naphthoquinone Lawsone activate AhR, both *in vitro* and *in vivo*. In human keratinocytes and epidermis equivalents, Lawsone exposure enhances the production of late epidermal proteins, impacts keratinocyte differentiation and proliferation, and regulates skin inflammation. To determine the potential use of Lawsone for therapeutic application, we harnessed human, murine and zebrafish models. In skin regeneration models, Lawsone interferes with physiological tissue regeneration and inhibits wound healing. Conversely, in a human acute dermatitis model, topical application of a Lawsone-containing cream ameliorates skin irritation. Altogether, our study reveals how a widely used natural plant pigment is sensed by the host receptor AhR, and how the physiopathological context determines beneficial and detrimental outcomes.

The skin acts as an important first barrier of the body, which is constantly exposed to diverse environmental and mechanical insults, such as pollution, infection, injury and radiation, amongst others<sup>1</sup>. Additionally, the application of cosmetics and other agents can have a major impact on skin homeostasis<sup>1</sup>. Among the most widely used skin dyes, are the extracts of *Lawsonia inermis*, commonly known as Henna<sup>2</sup>. In traditional medicine, Henna has been widely used to treat bacterial and fungal infections, inflammation, cancer and various skin pathologies<sup>3</sup>, but the underlying mechanisms remain insufficiently understood. Major side effects of Henna preparations are caused by the additive para-phenylenediamine (PPD) that has been associated with allergic contact dermatitis<sup>4,5</sup>. As natural product, Henna comprises a mixture of numerous compounds most of which are poorly characterized

<sup>1</sup>Department of Immunology, Max Planck Institute for Infection Biology, Charitéplatz 1, D-10117, Berlin, Germany. <sup>2</sup>Nuffield Department of Clinical Medicine, Ludwig Institute for Cancer Research, University of Oxford, Oxford, UK. <sup>3</sup>CEDOC, NOVA Medical School, NOVA University of Lisbon, Lisbon, 1169-056, Portugal. <sup>4</sup>Human Genomics Laboratory - University of Medicine and Pharmacy of Craiova, Craiova, Romania. <sup>5</sup>Leibniz-Forschungsinstitut fuer Molekulare Pharmakologie (FMP), Robert-Rössle-Strasse 10, 13125, Berlin, Germany. <sup>6</sup>Research Center of Gastroenterology and Hepatology, University of Medicine and Pharmacy of Craiova, Craiova, Romania. <sup>7</sup>Microarray Core Facility, Max Planck Institute for Infection Biology, Charitéplatz 1, D-10117, Berlin, Germany. <sup>8</sup>Biochemistry and Protein Purification Core Facility, Max Planck Institute for Infection Biology, Charitéplatz 1, D-10117, Berlin, Germany. <sup>9</sup>Laboratory of Immunoregulation and Immunopathology, INEM (Institut Necker-Enfants Malades), CNRS UMR8253, INSERM UMR1151 and Paris Descartes University, Paris, France. <sup>10</sup>Department of Dermatology and Allergy, Charité-Universitätsmedizin Berlin, Berlin, Germany. <sup>11</sup>Hagler Institute for Advanced Study, Texas A&M University, College Station, TX, USA. Laura Lozza and Pedro Moura-Alves contributed equally. Correspondence and requests for materials should be addressed to L.L. (email: [lozza@mpiib-berlin.mpg.de](mailto:lozza@mpiib-berlin.mpg.de)) or P.M.-A. (email: [pedro.mouraalves@ludwig.ox.ac.uk](mailto:pedro.mouraalves@ludwig.ox.ac.uk)) or S.H.E.K. (email: [kaufmann@mpiib-berlin.mpg.de](mailto:kaufmann@mpiib-berlin.mpg.de))

both chemically and functionally. The responsible pigment for the red colour after Henna application on skin, is the 1,4-naphthoquinone Lawsone, constituting 1–2% of the leaves<sup>6,7</sup>.

Recently, we unveiled that bacterial pigmented virulence factors, such as phenazines produced by *Pseudomonas aeruginosa* and the 1,4-naphthoquinone Phthiocol (Pht) from *Mycobacterium tuberculosis*, bind to and activate the Aryl Hydrocarbon Receptor (AhR), leading to AhR mediated immune defenses and detoxification of these virulence factors<sup>8</sup>. AhR is an evolutionarily conserved transcription factor widely expressed by almost all types of cells<sup>9–11</sup>. In its inactive state AhR resides in the cytoplasm in association with various chaperones. Upon activation, AhR binds to the AhR nuclear translocator (ARNT), and the resulting heterodimer induces the transcriptional regulation of multiple target genes, notably cytochrome P450 monooxygenases (*CYP1A1* and *CYP1B1*) and its own repressor, the AhR repressor (*AHRR*)<sup>11</sup>.

Earlier studies of AhR functions focused on detoxification of xenobiotic ligands such as benzo[a]pyrene, an ingredient of tobacco smoke<sup>12</sup> and the highly toxic 2,3,7,8-tetrachlorodibenzo-p-dioxin (TCDD)<sup>13</sup>. The list of ligands is continuously expanding, encompassing endogenous molecules (e.g. tryptophan (Trp), kynurenine or formylindolo[3,2-b] carbazole (FICZ)), dietary compounds and bacteria-derived ligands, and others (e.g. Itraconazole, Lipoxin A4, Prostaglandin G2 and Quercetin)<sup>8,14–18</sup>. In parallel with the increasing number of ligands, the biological functions attributed to this receptor are constantly growing rendering this receptor a ‘moving target’ of intense research<sup>14,19–21</sup>.

In the skin, AhR-mediated signals are critical in tissue regeneration, pathogenesis, inflammation and homeostasis<sup>9,22,23</sup> and AhR emerged as crucial player in the maintenance of skin integrity and immunity<sup>9,11</sup>. However, the outcome of AhR activation varies profoundly according to ligand properties, target cells and interactions with other signaling cascades<sup>22–25</sup>.

Here, we aimed to better characterize the effects of Lawsone, defining its mechanisms with an emphasis on skin, the central target tissue of Henna. We demonstrate that the main pigment of Henna, Lawsone, activates the AhR-transcriptional program and modulates skin homeostasis and recovery after external insult. We show that Lawsone inhibits proliferation, and accelerates differentiation of keratinocytes. Specifically, experiments with human skin equivalents, zebrafish and mice, reveal that Lawsone modulates tissue homeostasis and tissue regeneration, thereby interfering with the physiological process of wound healing. Despite its detrimental effect on wound healing, Lawsone’s capacity to reduce proliferation and promote keratinocyte differentiation, in parallel to modulation of skin inflammation, renders it a promising candidate for therapy of hyperproliferative skin diseases.

## Results

**Henna and lawsone activate the AhR pathway in keratinocytes.** AhR triggering depends on the quality and quantity of the activators as well as the intrinsic characteristics of the cell types<sup>11</sup>. Due to its similarity with known AhR ligands (Fig. 1A), such as TCDD and the mycobacterial pigment Pht<sup>8,24</sup>, we hypothesized that Lawsone, the main pigment from Henna, modulates AhR activity. *In silico* modeling studies predicted that all three molecules fit into the AhR binding pocket, albeit with different affinities (Figs 1B and Supplement 1A). The key residues Thr289, His291, Phe295, Ser365 and Gln383 are involved in forming hydrogen bonds with each of the three ligands. Lawsone has similar interactions as Pht. After rescoring, the free binding energy was as follows: TCDD ( $\Delta G_{\text{Bind}} -47.568$  kcal/mol), Pht ( $\Delta G_{\text{Bind}} -42.850$  kcal/mol) and Lawsone ( $\Delta G_{\text{Bind}} -38.591$  kcal/mol), with the lower value indicating a stronger binding in the ligand-receptor complex. Binding to AhR was confirmed in a previously established competition assay<sup>8</sup>, where Lawsone was able to displace radioactively labeled TCDD bound to AhR (Fig. Supplement 1B).

Keratinocytes are the most prominent cell type in the epidermis<sup>23</sup>, which constitute the first contact with external agents, including Henna<sup>7</sup>. We developed an AhR-luciferase reporter HaCaT (immortal human keratinocyte) cell line and measured AhR activation as readout of luciferase activity after stimulation. As can be seen in Fig. 1C, both TCDD and Pht induced AhR activation in keratinocytes. Similarly, Henna and the 1,4-naphthoquinone Lawsone also activated AhR (Fig. 1C). Dose-dependent AhR activation was further confirmed in other cell types, using the AhR-luciferase reporter THP-1 (human macrophage) cell line<sup>8</sup> (Fig. Supplement 1C). Extending our analysis to human primary keratinocytes (HEK cells), we evaluated whether the expression of AhR target genes was differentially regulated. *CYP1A1* was induced upon stimulation with both Henna and Lawsone (Fig. 1D). AhR dependency was confirmed using the specific AhR inhibitor, CH223191<sup>26</sup> (CH, Fig. 1D). *CYP1A1* transcription increased after stimulation with Henna containing 1  $\mu\text{M}$  of Lawsone, while it decreased at higher concentrations (Fig. 1D, left). Henna preparations contain several components, aside from Lawsone<sup>2</sup>, which would interfere with the kinetics of AhR activation. When cells were stimulated with Lawsone, *CYP1A1* was upregulated in a dose-dependent manner (Fig. 1D, right), without affecting cell viability (Fig. Supplement 1D–F). In keratinocytes obtained from different donors, *CYP1A1* and *AHRR* were consistently induced by Lawsone (Fig. 1E), Pht and TCDD (Fig. Supplement 1G). Notably, TLR2 stimulation (Pam2CSK4) did not activate AhR (Fig. Supplement 1G). Silencing of AhR in these cells by RNA interference (RNAi) was validated by Western Blotting (Fig. Supplement 1H), and led to reduced *CYP1A1* expression, further confirming that Lawsone induced *CYP1A1* in an AhR dependent manner (Figs 1E,G and Supplement 1I). Inhibition of *CYP1A1* can lead to indirect AhR activation in a mechanism involving Trp<sup>19,27</sup>. Using the EROD assay<sup>28</sup>, *CYP1A1* enzymatic activity was increased by Lawsone in HEK cells (Fig. 1H), as well as by the other ligands tested (Fig. Supplement 1J), thus excluding an indirect role of *CYP1A1* in AhR induction in this context.

To further validate our findings, we performed microarray analysis of HEK cells stimulated with Lawsone. We identified a set of AhR dependent genes (Table 1) and visualized the gene enrichment using receiver operating characteristic (ROC) curves<sup>29</sup>. A high score of the area under the curve and low q value indicate a significant and specific enrichment of AhR target genes upon stimulation with Lawsone (Figs 1I and Supplement 1K). Consistently, Ingenuity Pathway Analysis predicted the AhR canonical pathway amongst the top differentially regulated genes (Fig. Supplement 1L). Since *NQO1* can also be regulated by the transcription factor Nrf2<sup>30</sup>, we



Name	Gene	References
Cytochrome P450, family 1, member A1	CYP1A1	Hankinson, 1995; Katiyar <i>et al.</i> , 2000; Mukhtar <i>et al.</i> , 1986
Cytochrome P450, family 1, member B1	CYP1B1	Hankinson, 1995; Katiyar <i>et al.</i> , 2000; Mukhtar <i>et al.</i> , 1986
Aryl hydrocarbon receptor repressor	AHRR	Baba <i>et al.</i> , 2001; Frericks <i>et al.</i> , 2007
TCDD-inducible poly(ADP-ribose) polymerase	TIPARP	Lo and Matthews, 2012; Frericks <i>et al.</i> , 2007
Interleukin-1 $\beta$	IL-1 $\beta$	Sutter <i>et al.</i> , 1991
plasminogen activator inhibitor-2	PAI-2	Sutter <i>et al.</i> , 1991
epiregulin	EREG	Patel <i>et al.</i> , 2006
amphiregulin	AREG	Du <i>et al.</i> , 2005
insulin-like growth factor 1 receptor	IGFRI	Lo and Matthews, 2012
NAD(P)H:quinone oxidoreductase 1	NQO1	Wang <i>et al.</i> , 2013

**Table 1.** AhR dependent genes. The table includes AhR target genes containing the xenobiotic-responsive element (XRE) in the promoter region and genes described to be induced by AhR activation.

Name	Gene	Reference
glutamate-cysteine ligase, catalytic subunit	GCLC	Baird L., Arch Toxicol (2011) 85:241–272
NAD(P)H dehydrogenase, quinone 1	NQO1	
ferritin, light polypeptide	FTL	
glutathione S-transferase alpha 1	GSTA1	
glutathione S-transferase alpha 2	GSTA2	
glutathione S-transferase alpha 3	GSTA3	
glutathione S-transferase alpha 4	GSTA4	
glutathione S-transferase alpha 5	GSTA5	
glutathione S-transferase alpha 6, pseudogene	GSTA6P	
glutathione S-transferase alpha 7, pseudogene	GSTA7P	
glutathione S-transferase mu 1	GSTM1	
glutathione S-transferase mu 2 (muscle)	GSTM2	
glutathione S-transferase mu 3 (brain)	GSTM3	
glutathione S-transferase mu 4	GSTM4	
glutathione S-transferase mu 5	GSTM5	
glutathione S-transferase omega 1	GSTO1	
glutathione S-transferase omega 2	GSTO2	
glutathione S-transferase omega 3, pseudogene	GSTO3P	
glutathione S-transferase pi 1	GSTP1	
glutathione S-transferase theta 1	GSTT1	
glutathione S-transferase theta 2 (gene/pseudogene)	GSTT2	
glutathione S-transferase theta 2B (gene/pseudogene)	GSTT2B	
glutathione S-transferase zeta 1	GSTZ1	
hematopoietic prostaglandin D synthase	HPGDS	
aldo-keto reductase family 1, member A1 (aldehyde reductase)	AKR1A1	
aldo-keto reductase family 1, member B1 (aldose reductase)	AKR1B1	
aldo-keto reductase family 1, member B10 (aldose reductase)	AKR1B10	
aldo-keto reductase family 1, member B15	AKR1B15	
aldo-keto reductase family 1, member C1	AKR1C1	
aldo-keto reductase family 1, member C2	AKR1C2	
aldo-keto reductase family 1, member C3	AKR1C3	
aldo-keto reductase family 1, member C4	AKR1C4	
aldo-keto reductase family 1, member D1	AKR1D1	
aldo-keto reductase family 1, member E2	AKR1E2	
aldo-keto reductase family 7, member A2	AKR7A2	
aldo-keto reductase family 7, member A3 (aflatoxin aldehyde reductase)	AKR7A3	
potassium channel, voltage gated subfamily A regulatory beta subunit 1	KCNAB1	
potassium channel, voltage gated subfamily A regulatory beta subunit 2	KCNAB2	
potassium channel, voltage gated subfamily A regulatory beta subunit 3	KCNAB3	
ATP-binding cassette, sub-family C (CFTR/MRP), member 1	ABCC1	
Continued		

Name	Gene	Reference
ATP-binding cassette, sub-family C (CFTR/MRP), member 2	ABCC2	
ATP-binding cassette, sub-family C (CFTR/MRP), member 3	ABCC3	
ATP-binding cassette, sub-family C (CFTR/MRP), member 4	ABCC4	
ATP-binding cassette, sub-family C (CFTR/MRP), member 5	ABCC5	
ATP-binding cassette, sub-family C (CFTR/MRP), member 6	ABCC6	
ATP-binding cassette, sub-family C (CFTR/MRP), member 8	ABCC8	
ATP-binding cassette, sub-family C (CFTR/MRP), member 9	ABCC9	
ATP-binding cassette, sub-family C (CFTR/MRP), member 10	ABCC10	
ATP-binding cassette, sub-family C (CFTR/MRP), member 11	ABCC11	
ATP-binding cassette, sub-family C (CFTR/MRP), member 12	ABCC12	
ATP-binding cassette, sub-family C (CFTR/MRP), member 13, pseudogene	ABCC13	
cystic fibrosis transmembrane conductance regulator (ATP-binding cassette sub-family C, member 7)	CFTR	
UDP glucuronosyltransferase 1 family, polypeptide A complex locus	UGT1A	
UDP glucuronosyltransferase 1 family, polypeptide A1	UGT1A1	
UDP glucuronosyltransferase 1 family, polypeptide A2 pseudogene	UGT1A2P	
UDP glucuronosyltransferase 1 family, polypeptide A3	UGT1A3	
UDP glucuronosyltransferase 1 family, polypeptide A4	UGT1A4	
UDP glucuronosyltransferase 1 family, polypeptide A5	UGT1A5	
UDP glucuronosyltransferase 1 family, polypeptide A6	UGT1A6	
UDP glucuronosyltransferase 1 family, polypeptide A7	UGT1A7	
UDP glucuronosyltransferase 1 family, polypeptide A8	UGT1A8	
UDP glucuronosyltransferase 1 family, polypeptide A9	UGT1A9	
UDP glucuronosyltransferase 1 family, polypeptide A10	UGT1A10	
UDP glucuronosyltransferase 1 family, polypeptide A11 pseudogene	UGT1A11P	
UDP glucuronosyltransferase 1 family, polypeptide A12 pseudogene	UGT1A12P	
UDP glucuronosyltransferase 1 family, polypeptide A13 pseudogene	UGT1A13P	
UDP glucuronosyltransferase 2 family, polypeptide A1, complex locus	UGT2A1	
UDP glucuronosyltransferase 2 family, polypeptide A2	UGT2A2	
UDP glucuronosyltransferase 2 family, polypeptide A3	UGT2A3	
UDP glucuronosyltransferase 2 family, polypeptide B4	UGT2B4	
UDP glucuronosyltransferase 2 family, polypeptide B7	UGT2B7	
UDP glucuronosyltransferase 2 family, polypeptide B10	UGT2B10	
UDP glucuronosyltransferase 2 family, polypeptide B11	UGT2B11	
UDP glucuronosyltransferase 2 family, polypeptide B15	UGT2B15	
UDP glucuronosyltransferase 2 family, polypeptide B17	UGT2B17	
UDP glucuronosyltransferase 2 family, polypeptide B24 pseudogene	UGT2B24P	
UDP glucuronosyltransferase 2 family, polypeptide B25 pseudogene	UGT2B25P	
UDP glucuronosyltransferase 2 family, polypeptide B26 pseudogene	UGT2B26P	
UDP glucuronosyltransferase 2 family, polypeptide B27 pseudogene	UGT2B27P	
UDP glucuronosyltransferase 2 family, polypeptide B28	UGT2B28	
UDP glucuronosyltransferase 2 family, polypeptide B29 pseudogene	UGT2B29P	
UDP glycosyltransferase 3 family, polypeptide A1	UGT3A1	
UDP glycosyltransferase 3 family, polypeptide A2	UGT3A2	
UDP glycosyltransferase 8	UGT8	

**Table 2.** Nrf2-related genes. The table includes Nrf2 target genes.

extended our analysis to the enrichment of genes associated with this pathway (Table 2). The area under the curve indicates that Nrf2-related genes were less enriched compared to AhR-related genes (Fig. Supplement 1M,N), pointing to a preferential activation of AhR. In summary, our results demonstrate that the 1,4-naphthoquinone Lawsone, the critical pigment in Henna, binds and activates the AhR pathway in keratinocytes. While the effects of Henna may be confounded by other components in the extract, Lawsone specifically activates AhR without causing cell toxicity, at least at the conditions tested.

**Lawsone stimulation modulates keratinocyte proliferation and differentiation.** The AhR pathway impacts on epidermal differentiation, and the consequences of AhR activation considerably depend on the properties of the ligands and the target cells<sup>22,25,31,32</sup>. As demonstrated in Fig. 2A, Lawsone inhibited keratinocyte proliferation. Furthermore, microarray analysis of HEK cells stimulated with Lawsone pointed to a skewing towards differentiation (Fig. Supplement 2A). ROC curve analysis of genes of the epidermal differentiation

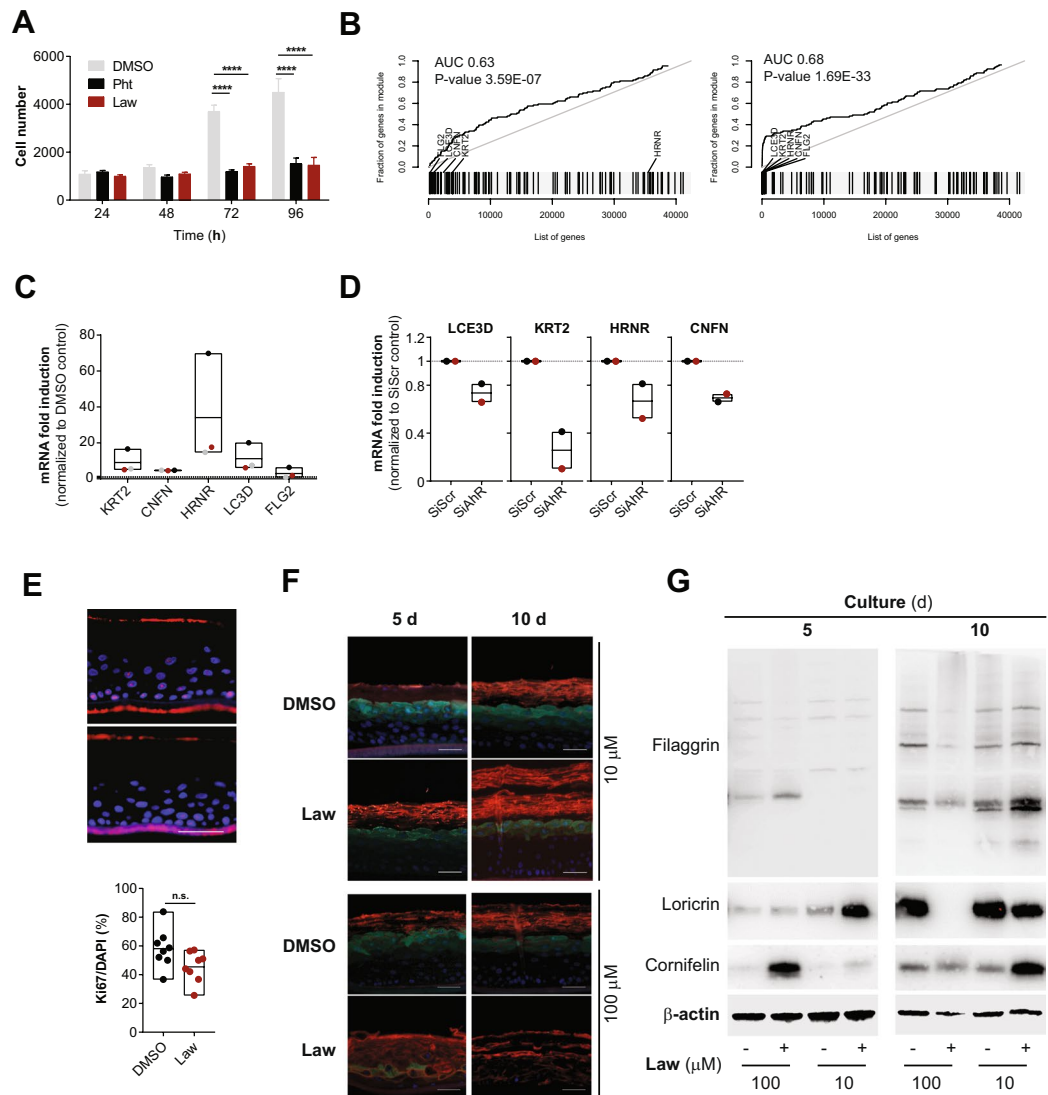


**Figure 2.** Lawsone stimulation modulates keratinocyte proliferation and differentiation. **(A)** Nuc red Live 647 positive HEK cells at different time points after stimulation with Lawsone (Law, 10  $\mu$ M) and Phthiocol (Pht, 50  $\mu$ M), compared to DMSO. **(B)** Epidermal differentiation complex and keratin gene enrichment of HEK cells after Lawsone stimulation (10  $\mu$ M) and relative to TLR2 stimulation (Pam2CSK4, 0.236  $\mu$ M) at (left) 4h and (right) 24h. Area under the curve (AUC), q-value and highly enriched genes are indicated. **(C)** *KRT2*, *CNFN*, *HRNR*, *LCE3D* and *FLG2* expression of HEK cells after 24h stimulation with Lawsone (10  $\mu$ M) normalized to DMSO. Each color depicts results of the same individual. **(D)** *LCE3D*, *KRT2*, *HRNR* and *CNFN* expression on HEK cells transfected with AhR-siRNA (siAhR) or Scramble control (siScr) and further stimulated for 24h with Lawsone (10  $\mu$ M). Values are relative to siScr. Each color depicts results of the same individual. **(E, top)** Epidermal skin equivalents were stimulated for 5d with Lawsone (10  $\mu$ M) or DMSO and stained with DAPI (blue) and the proliferation marker KI67 (purple). **(E, bottom)** Percentage of KI67 positive cells normalized to the total number of cells (DAPI). **(F)** Representative of an *in vitro* epidermis model experiment stained for Cornifelin (red) and Loricrin (green) and **(G)** protein expression of Filaggrin, Cornifelin and Loricrin at day 5 or 10 of culture after stimulation with 10 or 100  $\mu$ M of Lawsone (blots were cropped from the same gel. Full unedited gels are provided in Supplementary Data). **(A, C)** Data from 3 independent experiments are shown. **(D)** Data from 2 independent donors. **(E top, F, G)** One representative experiment out of 2 is shown. **(E)** Pooled data from 2 different experiments is shown. **(A)** Mean + S.E.M., **(C–E bottom)** Floating bars, Mean Min to Max. **(A)** Two-way ANOVA with Fisher's test, **(C)** One-way ANOVA with Dunn's test. **(E, bottom)** Student's t-test. \* $P < 0.05$ ; \*\* $P < 0.01$ , \*\*\* $P < 0.001$ , \*\*\*\* $P < 0.0001$ .

complex (EDC), and family I and II keratins (Table 3) revealed a significant enrichment upon Lawsone stimulation (Fig. 2B). This was mainly due to upregulation of the genes involved in formation of the cornified envelope (Supplementary Dataset File 1). Cornifelin (CNFN), hornerin (HRNR), late cornified envelope 3D (LCE3D), keratin 2 (KRT2) and filaggrin 2 (FLG2) are critical for epidermal differentiation<sup>33,34</sup>. qRTPCR analysis confirmed the induction of these genes in HEK cells upon Lawsone exposure (Fig. 2C). Thus, Lawsone modulates the expression of genes involved in cornified envelope generation.

	approved symbol	approved name	categories	References
Keratin type I	KRT9	keratin 9, type I	Human type I epithelial keratins	Schweizer <i>et al.</i> , 2006; <a href="http://www.genecards.org/">http://www.genecards.org/</a>
	KRT10	keratin 10, type I	Human type I epithelial keratins	
	KRT12	keratin 12, type I	Human type I epithelial keratins	
	KRT13	keratin 13, type I	Human type I epithelial keratins	
	KRT14	keratin 14, type I	Human type I epithelial keratins	
	KRT15	keratin 15, type I	Human type I epithelial keratins	
	KRT16	keratin 16, type I	Human type I epithelial keratins	
	KRT17	keratin 17, type I	Human type I epithelial keratins	
	KRT18	keratin 18, type I	Human type I epithelial keratins	
	KRT19	keratin 19, type I	Human type I epithelial keratins	
	KRT20	keratin 20, type I	Human type I epithelial keratins	
	KRT23	keratin 23, type I	Human type I epithelial keratins	
	KRT24	keratin 24, type I	Human type I epithelial keratins	
	KRT25	keratin 25, type I	Human type I epithelial keratins	
	KRT26	keratin 26, type I	Human type I epithelial keratins	
	keratin type II	KRT1	keratin 1, type II	
KRT2		keratin 2, type II	Human type II epithelial keratins	
KRT3		keratin 3, type II	Human type II epithelial keratins	
KRT4		keratin 4, type II	Human type II epithelial keratins	
KRT5		keratin 5, type II	Human type II epithelial keratins	
KRT6A		keratin 6A, type II	Human type II epithelial keratins	
KRT6B		keratin 6B, type II	Human type II epithelial keratins	
KRT6C		keratin 6C, type II	Human type II epithelial keratins	
KRT7		keratin 7, type II	Human type II epithelial keratins	
KRT8		keratin 8, type II	Human type II epithelial keratins	
KRT71		keratin 71, type II	Human type II epithelial keratins	
KRT72		keratin 72, type II	Human type II epithelial keratins	
KRT73		keratin 73, type II	Human type II epithelial keratins	
KRT74		keratin 74, type II	Human type II epithelial keratins	
KRT75		keratin 75, type II	Human type II epithelial keratins	
KRT76		keratin 76, type II	Human type II epithelial keratins	
KRT77	keratin 77, type II	Human type II epithelial keratins		
KRT78	keratin 78, type II	Human type II epithelial keratins		
KRT79	keratin 79, type II	Human type II epithelial keratins		
KRT80	keratin 80, type II	Human type II epithelial keratins		
non epidermal differentiation complex-associated	CNFN	Cornifelin		Kennedy <i>et al.</i> , 2013
epidermal differentiation complex	CRNN	Cornulin		Mischke <i>et al.</i> , 1996; Kyriotou <i>et al.</i> , 2012
	FLG	Filaggrin		
	FLG2	Filaggrin Family Member 2		
	HRNR	Hornerin		
	IVL	Involucrin		
	LCE1A	Late Cornified Envelope 1A		
	LCE1B	Late Cornified Envelope 1B		
	LCE1C	Late Cornified Envelope 1C		
	LCE1D	Late Cornified Envelope 1D		
	LCE1E	Late Cornified Envelope 1E		
	LCE1F	Late Cornified Envelope 1F		
	LCE2A	Late Cornified Envelope 2A		
	LCE2B	Late Cornified Envelope 2B		
	LCE2C	Late Cornified Envelope 2C		
	LCE2D	Late Cornified Envelope 2D		
	LCE3A	Late Cornified Envelope 3A		
LCE3B	Late Cornified Envelope 3B			
LCE3C	Late Cornified Envelope 3C			
LCE3D	Late Cornified Envelope 3D			
Continued				

approved symbol	approved name	categories	References
LCE3E	Late Cornified Envelope 3E		
LCE4A	Late Cornified Envelope 4A		
LCE5A	Late Cornified Envelope 5A		
LCE6A	Late Cornified Envelope 6A		
LEP7	Late Envelope Protein 7		
LOR	Loricrin		
NICE-1	Cysteine-Rich C-Terminal 1		
RPTN	Repetin		
S100A1	S100 Calcium Binding Protein A1		
S100A2	S100 Calcium Binding Protein A2		
S100A3	S100 Calcium Binding Protein A3		
S100A4	S100 Calcium Binding Protein A4		
S100A5	S100 Calcium Binding Protein A5		
S100A6	S100 Calcium Binding Protein A6		
S100A7	S100 Calcium Binding Protein A7		
S100A8	S100 Calcium Binding Protein A8		
S100A9	S100 Calcium Binding Protein A9		
S100A10	S100 Calcium Binding Protein A10		
S100A11	S100 Calcium Binding Protein A11		
S100A12	S100 Calcium Binding Protein A12		
S100A13	S100 Calcium Binding Protein A13		
S100A14	S100 Calcium Binding Protein A14		
S100A15	S100 Calcium Binding Protein A15		
S100A16	S100 Calcium Binding Protein A16		
S100A7L2	S100 Calcium Binding Protein A7-Like 2		
SPRR1A	small proline-rich proteins 1A		
SPRR1B	small proline-rich proteins 1B		
SPRR2A	small proline-rich proteins 2A		
SPRR2B	small proline-rich proteins 2B		
SPRR2C	small proline-rich proteins 2C		
SPRR2D	small proline-rich proteins 2D		
SPRR2E	small proline-rich proteins 2E		
SPRR2F	small proline-rich proteins 2F		
SPRR2G	small proline-rich proteins 2G		
SPRR3	small proline-rich proteins 3		
SPRR4	small proline-rich proteins 4		
THH	Trichohyalin		
THHL1	Trichohyalin-Like 1		

**Table 3.** Epidermal differentiation complex and keratin genes. The table includes genes of the epidermal differentiation complex and keratins.

Epidermal differentiation occurs after activation of the AP-1 transcription factor<sup>35</sup>. To interrogate whether epidermal differentiation requires AP-1 activity, keratinocytes were stimulated with Lawsonine in the presence of the AP-1 inhibitor tanshinone IIA (TIIA)<sup>36</sup>. Efficient blocking of AP-1 activity was shown by inhibition of CSF3 expression (Fig. Supplement 2B)<sup>36</sup>. Lawsonine induced upregulation of *CNFN*, *HRNR*, *LCE3D* and *KRT2* (Fig. Supplement 2C), and of the AhR-target genes *CYP1A1* and *AHRR* even in presence of TIIA indicating an AP-1 independent activation. Moreover, inhibiting AhR by RNAi reduced expression of these genes upon Lawsonine



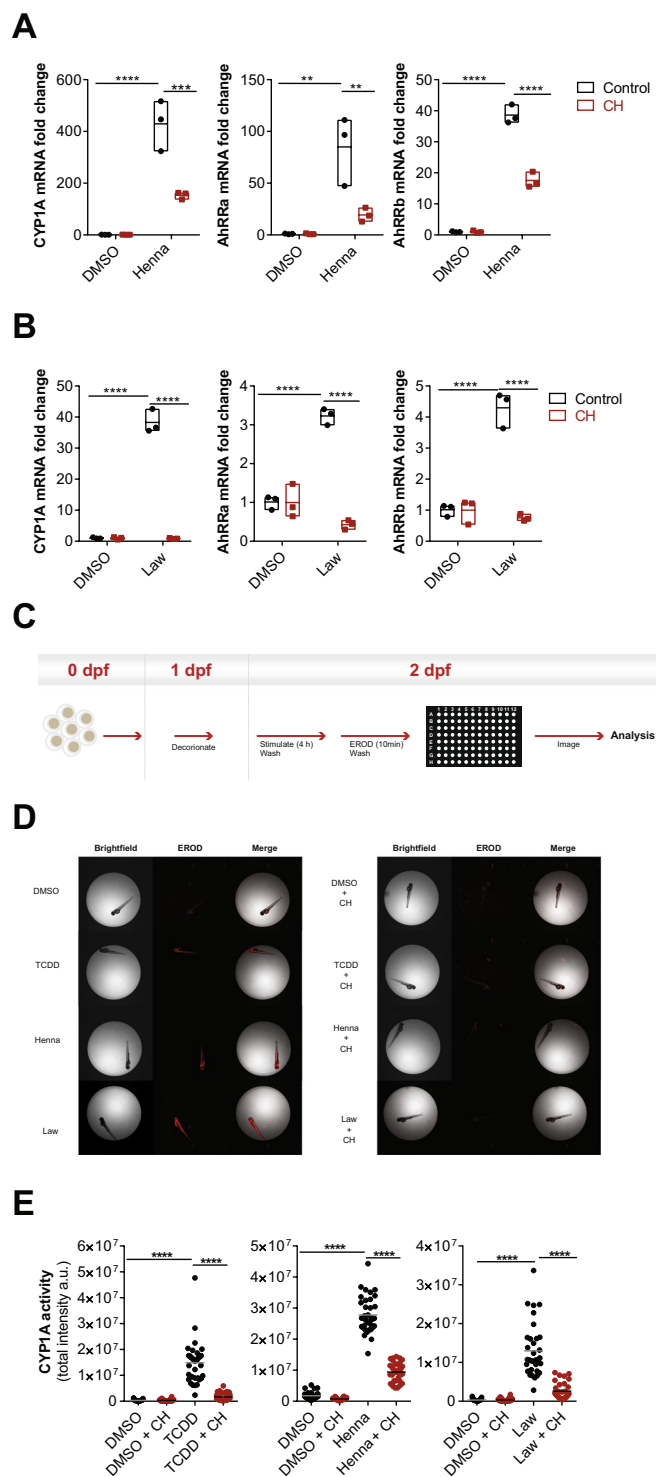


**Figure 3.** Henna and Lawsone activate AhR in zebrafish larvae. **(A,B)** Fold induction of *CYP1A*, *AhRRa* and *AhRRb* transcripts from zebrafish larvae (2 days post-fertilization, dpf) treated (red squares) or not (black circles) for 2 h with 5  $\mu$ M of AhR inhibitor CH223191, followed by further 4 h stimulation with **(A)** Henna (equivalent to 10  $\mu$ M Lawsone), **(B)** Lawsone (10  $\mu$ M) or DMSO vehicle control. Triplicates of 12 larvae depicted in each data point. **(C)** Scheme of the semi-high throughput experimental design developed to measure zebrafish larvae *CYP1A* enzymatic activity. **(D)** Representative images obtained upon *CYP1A* activity measurements using an Array Scan TM XTI Live High Content Platform. **(E)** *CYP1A* enzymatic activity expressed as total intensity of resorufin detected per larva (each dot represents one larva). 1 representative experiment out of 3 are shown ( $n = 36$  larvae per condition). **(A,B)** Data from 1 representative experiment out of 3 is shown. **(A,B)** Floating bars, Mean Min to Max. **(A,B)** Two-way ANOVA with Bonferroni's test. **(E)** Two-way ANOVA with Fisher's test. \*\* $P < 0.01$ , \*\*\* $P < 0.001$ , \*\*\*\* $P < 0.0001$ .

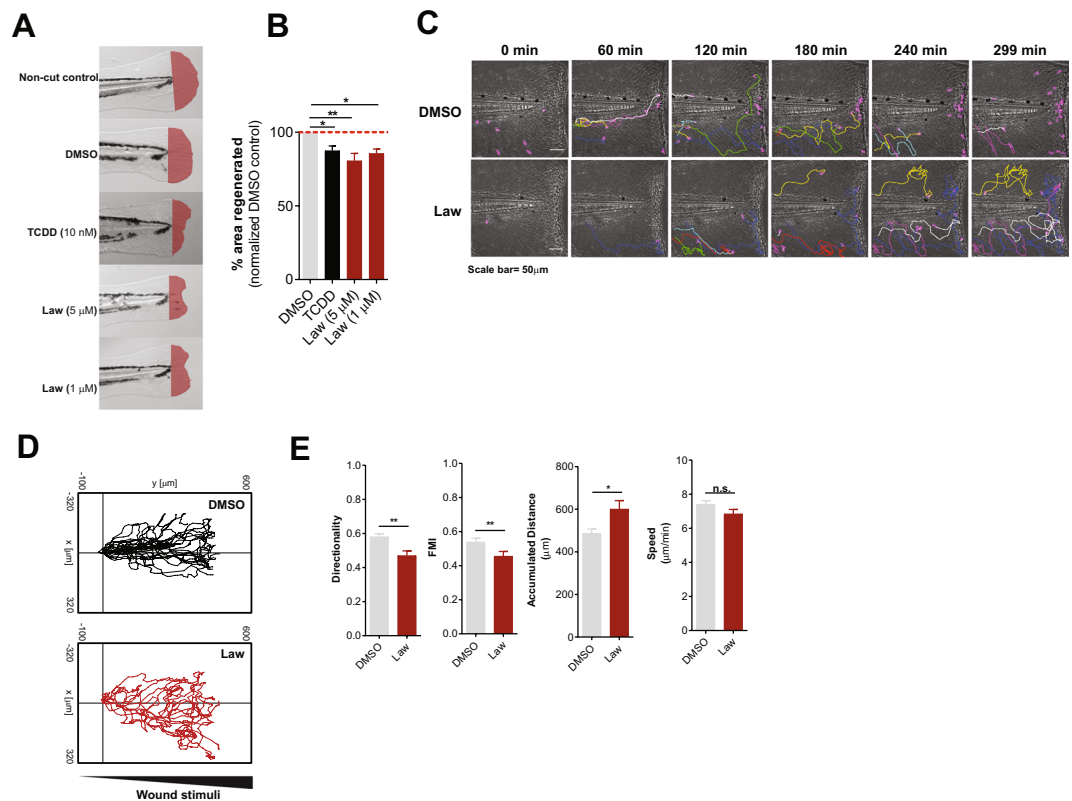


**Figure 4.** Lawsone inhibits wound healing and skin regeneration *in vivo*. **(A)** Representative images of zebrafish fin regeneration 3 days post amputation (dpa) and exposure to different stimuli. Regenerated area depicted in red. **(B)** Quantification of the zebrafish tail fin area regenerated, normalized to DMSO treated larvae. **(C)** Neutrophil migration to zebrafish tailfin wounds visualized in DMSO or Lawsone-treated transgenic larvae Tg(mpeg.mCherryCAAX SH378 mpx:GFP i114). Frames from representative movies of migrating leukocytes in the wounded tail fin are shown. The lines indicate tracking of individual neutrophils over the indicated time point of the experiment. Wound is represented with a white dashed line. **(D)** 2D tracks of individual neutrophils migrating in the tail fin of wounded neutrophil-GFP zebrafish 3dpf larvae exposed to 10 μM Lawsone (n = 8) or DMSO (n = 23). **(E)** Quantification of 2D directionality, Forward migration index (FMI), accumulated distance and speed of individual leukocytes in the wounded tailfin. **(B)** Pooled data from 4 independent experiments with at least 24 larvae per condition per experiment, Mean + S.E.M., **(E)** Data from 2 pooled experiments, Mean + S.E.M. **(B)** One-way ANOVA with Fisher's test, **(E)** Student's t-test. \*P < 0.05; \*\*P < 0.01; \*\*\*P < 0.001; n.s.-not significant.

exposure (Fig. 2D). Thus, Lawsone requires AhR activation to induce the expression of genes involved in the formation of the cornified envelope independently of AP-1 activity.

To validate our findings, we treated fresh skin biopsies from individuals after skin surgical excision with Lawsone and confirmed the upregulation of *CYP1A1* and *AHRR* (Fig. Supplement 2E), but not of *KRT2*, *CNFN*, *FLG* and *LCE3D* (Fig. Supplement 2E). We reasoned that fully differentiated skin obtained in biopsies may mask subtle differences of Lawsone on epidermal layers containing proliferating keratinocytes. Hence, we visualized epidermal differentiation over time in human epidermis equivalent models<sup>23,34</sup>. Keratinocytes were treated daily with Lawsone, and tissue differentiation was analyzed after 5 or 10 days of culture (Fig. Supplement 2F). As shown in Fig. 2E, the percentage of Ki67 positive cells after 5 days of treatment was slightly reduced, although not significantly, pointing to inhibition of proliferation, as observed *in vitro* (Fig. 2A). Importantly, treatment with 10 μM Lawsone increased the thickness of the *stratum corneum* after 5 and 10 days (Fig. 2F) and correlated with higher expression of loricrin (at 5 days), cornifelin (at 10 days) and filaggrin (at 10 days) measured by immunofluorescence and Western blotting (Fig. 2F,G). At higher concentrations, Lawsone further boosted the differentiation of the *stratum corneum* resulting in a disorganized epidermal structure (Fig. 2F). Hence, Lawsone impacts epidermal differentiation in human skin.

#### Lawsone activates the AhR pathway in zebrafish larvae and modulates tissue regeneration.

In order to further evaluate consequences of Lawsone exposure during tissue regeneration *in vivo*, we took advantage of a previously established zebrafish model<sup>37–39</sup>. This model organism has been extensively used in toxicology, including studies with AhR<sup>37</sup>, as well as in skin wound healing and re-epithelization studies<sup>38,40</sup>. The epidermis and dermis layers occur in zebrafish larvae as early as 1 day post fertilization (dpf)<sup>40</sup>. 2dpf larvae were exposed to Henna and Lawsone for 4 hours and AhR dependent gene expression was evaluated (Fig. Supplement 3A).

Zebrafish express three isoforms of AhR (*AHR1a*, *AHR1b* and *AHR2*)<sup>37,39</sup> and 2 isoforms of AhRR (*AHRRa* and *AHRRb*)<sup>40</sup>. As in humans, the expression of *CYP1A*, as well as the repressors *AHRRa* and *AHRRb*, are regulated in an AhR dependent manner<sup>39</sup>. The expression of the three genes was increased upon stimulation with Henna, Lawsone (Fig. 3A,B) or TCDD (Fig. Supplement 3B). Gene induction was reversed by the AhR inhibitor, validating AhR dependency. Similar to human cells (Figs 1H and Supplement 1J), larvae exposed to TCDD, Henna or Lawsone increased CYP1A enzymatic activity (Fig. 3C–E), which was reversed by CH223191 (Figs 3D,E and Supplement 3C). Under these conditions, no toxicity was observed (Fig. Supplement 3D). Thus, these *in vivo* results further substantiate our *in vitro* findings demonstrating that Lawsone activates AhR signaling.

We then performed tail fin regeneration assays and found that fin regeneration was inhibited in the presence of Lawsone (Figs 4A,B, Supplement 4A) as observed previously with Dioxin<sup>41,42</sup>. Tissue damage induces the early recruitment of leukocytes to restore barrier integrity and tissue homeostasis, which critically determines the regenerative outcome<sup>43</sup>. Using a transgenic zebrafish line expressing GFP-labeled neutrophils (mpeg.mCherry-CAAX SH378 mpx:GFP i114)<sup>44,45</sup> we observed that upon exposure of the tailfin wound to Lawsone, neutrophils moved (i) more randomly, (ii) for longer distances and (iii) with decreased directionality, as compared to controls (Figs 4C–E, Supplement 4B and Movie Supplement 1). Moreover, neutrophils continued to patrol around in a “zig-zag” fashion and were not arrested at the wound (Fig. 4C,D and Movie Supplement 1). Notably, Lawsone exposure did not affect the speed of mobilizing cells (Fig. 4E). We conclude that Lawsone inhibits early steps of tissue regeneration by affecting physiological leukocyte attraction.

We extended our studies to a mouse wound healing model<sup>46</sup>. Application of 10  $\mu$ M of Lawsone on the wound for 5 consecutive days delayed wound healing (Fig. Supplement 4C,D). In sum, Lawsone interferes with the natural process of wound healing in different models.

**Lawsone ameliorates skin recovery in a model of contact skin irritation.** Besides the induction of genes of epidermal differentiation, the analysis of keratinocytes stimulated with Lawsone revealed that genes related to psoriasis, dermatitis and inflammation were also affected (Table 4). Accordingly, we evaluated whether Lawsone ameliorates skin disorders characterized by irritation, inflammation and epidermal hyper-proliferation, in a human model of acute irritant contact dermatitis<sup>47</sup>. Skin irritation was induced by a single application of 30  $\mu$ L of 5% sodium dodecyl sulfate (SDS) using self-adhesive patches which had been identified as reliable dose to induce an irritant contact dermatitis<sup>47</sup>. Lawsone was dissolved in base cream at different concentrations (0.5%, 1%, and 3%) and topically applied on the skin of the forearm of healthy volunteers 24 h upon exposure to SDS. Images of the irritation spot and blood flux were taken daily. Decreased intensity of the flux was detected upon exposure to Lawsone, with slight differences between the concentrations and individuals tested (Fig. 5A,B). Time dependent resolution of irritation was observed in all individuals, but a strikingly faster reduction in blood flux was detected upon Lawsone exposure (Fig. 5C). Thus, Lawsone dose dependently inhibits human skin responses to irritation suggesting that detrimental or beneficial effects of Lawsone on the skin depend not only on its intrinsic nature but also on the context of skin (dys)function.

## Discussion

Despite the widespread use of the Henna plant *Lawsonia inermis* as a cosmetic dye for hair and skin, and its broad exploitation in traditional medicine due to assumed beneficial effects, little is known about the underlying mechanisms and role of its essential pigment, Lawsone<sup>2</sup>.

In our study, Lawsone emerged as an AhR ligand, directly binding to this receptor and eliciting AhR dependent responses in different *in vitro* and *in vivo* models. Moreover, we demonstrated that Lawsone interferes with the physiological skin regeneration processes. Lawsone modulated epidermal cell proliferation and differentiation in the skin, profoundly affecting wound healing. Nevertheless, in acute irritant contact dermatitis, Lawsone ameliorated irritation and accelerated healing.

In the skin, AhR plays a fundamental role in the maintenance of skin integrity in face of continuous environmental insults<sup>25</sup> and the outcome of its activation is fine-tuned by the interplay of the individual ligand properties and the physiological state of the skin<sup>25</sup>. Exposure to Lawsone induced the expression of AhR dependent genes not only in human primary keratinocytes and keratinocytic cell lines, but also in zebrafish larvae and human skin biopsies. AhR dependency was validated by RNAi and by using the pharmacologic AhR inhibitor CH223191. Activation of AhR can be related to inhibition of CYP1A1 activity, increasing expression of Trp metabolites activating AhR<sup>19</sup>. Here, Lawsone did not inhibit the enzymatic activity of CYP1A, neither in zebrafish nor in human keratinocytes.

AhR has been shown to affect epidermal differentiation<sup>22,34</sup>. Under homeostatic conditions, AhR KO mice suffer from impaired barrier formation with enhanced transepidermal water loss and reduced expression of proteins involved in epidermal differentiation<sup>22,32</sup>. Similar results were obtained after exposure of keratinocytes to AhR antagonists<sup>22</sup>, pointing to an essential role of the AhR in the physiological development of the skin barrier. Accordingly, endogenous Trp metabolites (e.g. FICZ) modulate keratinocyte functions and differentiation<sup>15</sup>, while exogenous AhR-activators such as TCDD upregulate genes of epidermal differentiation<sup>33,48,49</sup>. Although FICZ and TCDD are both high-affinity AhR ligands, TCDD resists Cyp1-mediated degradation<sup>13</sup>, while FICZ is efficiently degraded<sup>50</sup>, suggesting that both ligand affinity and stability, shape the action on target cells. Consistent with this, TCDD favors keratinocyte differentiation but also gives rise to chloracne in overexposed humans<sup>51</sup>, characterized by the appearance of pustules and cysts in the skin<sup>52</sup>. Constitutive AhR activation in keratinocytes also causes inflamed skin lesions<sup>53</sup>. Hence, depending on ligand and context, AhR modulation can act as a “double-edged sword”, leading to beneficial or detrimental outcomes on skin regeneration.

In our studies, Lawsone differentially regulated distinct genes and proteins involved in keratinocyte differentiation. In agreement, proliferation of primary keratinocytes in a human organotypic skin model was decreased. Notably, the expression of specific keratinocyte differentiation genes upon Lawsone exposure was

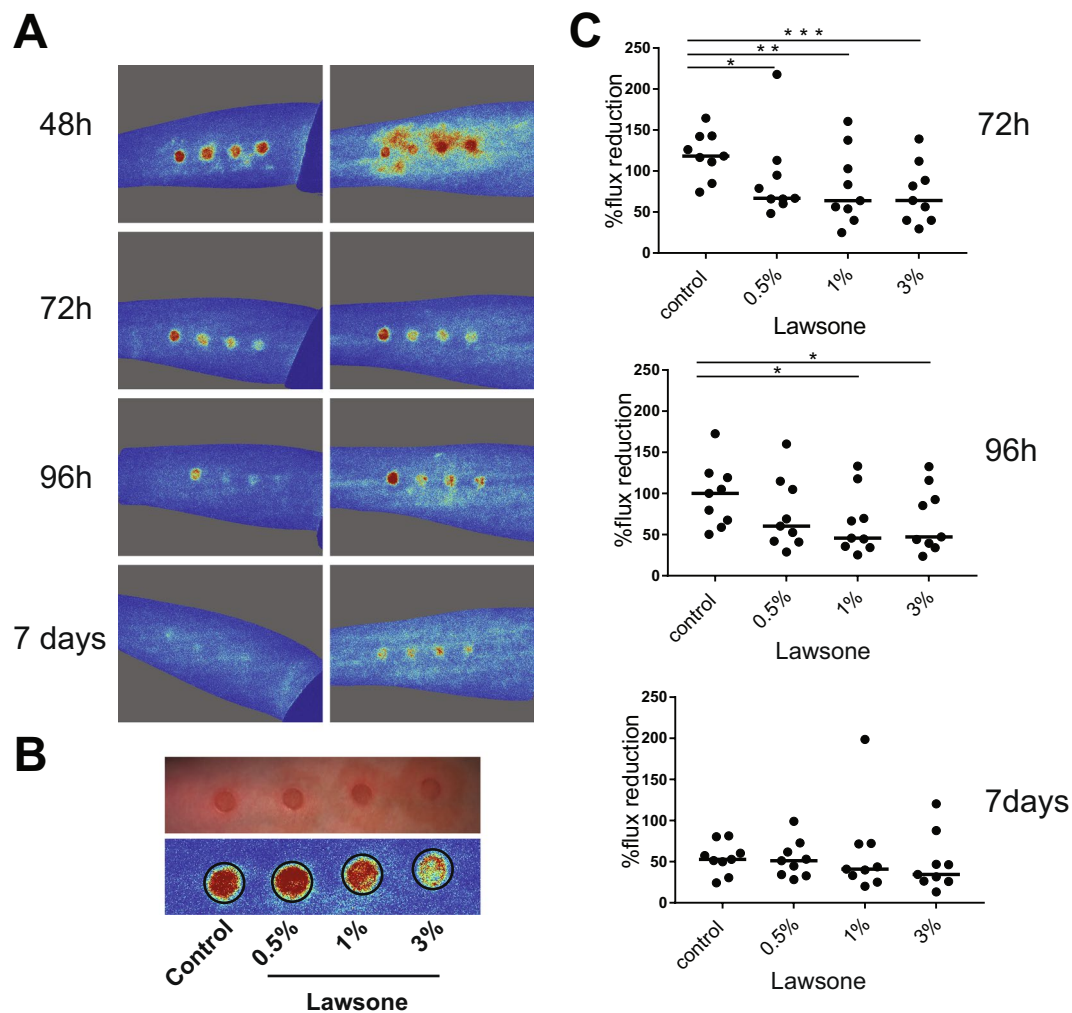


**Figure 5.** Lawsone ameliorates skin recovery in a model of human contact skin irritation. **(A)** Representative images of blood flux measured using the MoorFLPI-2 Full\_Field Laser Perfusion Imager V1.1 software at 48–72–96 h and 7 days upon application of 0.5% SDS. Cream containing increasing concentration of Lawsone (% of Lawsone = weight of Lawsone (g) per 100 g of cream) was applied 24 h after SDS treatment. **(B)** Example of (top) irritation spots and (bottom) blood flux quantification. After SDS application all individuals were treated as follow: far left: control cream, left: 0.5%; right 1%; far right 3% Lawsone cream. **(C)** Percentage of flux reduction at different time points normalized to the respective average flux intensity measured at 48 h post-SDS application. **(A)** Representative responses of 2 out of 9 volunteers are shown. **(C)** Data from 9 individuals are shown. One-way ANOVA with Fisher's test. \* $P < 0.05$ ; \*\* $P < 0.01$ ; \*\*\* $P < 0.001$ .

AhR dependent. Although Lawsone did not affect survival of keratinocytes, high concentrations profoundly shuffled the epidermal layers, giving rise to a thick and fragile cornified structure. Cell proliferation in regenerating zebrafish larval caudal fins in response to Dioxin has been shown to decrease<sup>42</sup>. Similarly, here we showed that Lawsone impairs zebrafish larval fin regeneration. Moreover, wound healing experiments in zebrafish and mouse models revealed a delay in this process caused by Lawsone. In sum, different *in vitro* (cell lines and human skin model) and *in vivo* (mouse and zebrafish) approaches conclusively demonstrate that Lawsone impacts tissue proliferation, differentiation and regeneration.

AhR mediated effects can result from different interactions between this receptor and other intracellular signaling pathways, such as Nrf2<sup>11,54</sup>. Here, we showed that Lawsone upregulated the expression of the antioxidant enzyme *NQO1*, a gene also regulated by Nrf2. Nrf2 is known to protect against reactive oxygen species<sup>30,54</sup> and AhR and Nrf2 interactions were found crucial for the cytoprotective effects of the fungicide ketoconazole in keratinocytes<sup>55</sup>. In our microarray analyses, AhR dependent responses were induced more profoundly, and occurred earlier, than Nrf2 responses suggesting an important role of AhR in initiating cell responses. Yet, it is tempting to speculate that some of the elicited effects on skin may involve AhR and other molecules, such as Nrf2.

Chronic inflammatory skin disorders emerge as outcome of diverse environmental and immune factors, and diseases such as psoriasis and atopic dermatitis are characterized by dysbalanced AhR signaling. Accordingly, therapeutic interventions by AhR-targeting strategies have been suggested<sup>25,33,36</sup>. For example, coal tar has been widely used for treatment of atopic dermatitis and was shown to induce AhR dependent responses in the skin<sup>34</sup>. Coal tar is composed of

Symbol	logFc. (Law vs DMSO at 24 h)	p-value
IFIT1	-2,58	5,53E-21
MX1	-2,31	9,39E-17
ISG15	-2,20	3,06E-17
ISG15	-2,19	3,06E-17
IFIT3	-1,69	3,19E-13
IFI6	-1,66	7,69E-17
IFI44	-1,54	1,29E-12
EPSTI1	-1,44	1,36E-11
IFNK	-1,24	4,32E-10
TOP2A	-1,22	2,13E-10
IFIH1	-1,20	3,84E-11
PPP1R3C	-1,20	1,44E-10
SAMD9L	-1,12	3,91E-07
IGFBP3	-1,10	3,71E-13
PARP9	-1,10	6,15E-09
PARP9	-1,10	6,15E-09
MKI67	-1,08	5,65E-10
OAS2	-1,07	1,70E-05
SOCS1	-1,02	3,30E-10
EFNB2	-1,01	1,65E-07
OAS1	-0,99	3,67E-07
CTSL2	-0,98	1,34E-07
DDX58	-0,97	9,52E-05
IRF9	-0,97	2,64E-07
PDK4	-0,95	0,000375155
SYNE2	-0,95	6,10E-06
CSPG4	-0,92	3,75E-09
SGK1	-0,92	2,15E-09
IFI44L	-0,90	3,19E-05
EIF2AK2	-0,89	2,34E-05
RTP4	-0,88	2,53E-06
KRT15	-0,87	9,02E-05
SPC25	-0,87	9,74E-08
ANXA1	-0,85	1,61E-08
LAMP3	-0,85	2,63E-09
CAV1	-0,84	0,00298468
CCL27	-0,82	1,16E-06
DSG1	-0,81	4,72E-08
SP100	-0,81	4,12E-06
STAT1	-0,79	2,37E-09
TAGLN	-0,78	1,02E-05
GJB2	-0,78	2,33E-05
PBK	-0,78	4,38E-07
CCNA2	-0,77	3,25E-08
TIMP3	-0,77	4,81E-07
ANXA2	-0,75	0,000797819
GBP2	-0,73	3,67E-06
IL15	-0,72	2,30E-05
AHNAK	-0,71	0,005674451
JUN	-0,70	9,43E-08
ID4	-0,70	0,000169748
IL33	-0,68	0,000121647
TLR3	-0,68	2,94E-05
OPTN	-0,67	8,05E-07
SLC6A2	-0,67	8,47E-06
JAK2	-0,66	0,009480402
NR3C1	-0,65	9,22E-05
PTRF	-0,64	1,47E-07
BLNK	-0,64	0,000567571
Continued		

Symbol	logFc. (Law vs DMSO at 24h)	p-value
CAMK2N1	-0,63	5,82E-06
P4HA2	-0,63	0,019848721
FGF7	-0,63	0,00122151
IFIT5	-0,60	4,69E-06
MX2	-0,58	0,003413461
USP18	-0,53	4,04E-05
TRIM21	-0,53	0,012172344
OAS3	-0,52	0,002218834
ITSN2	-0,47	0,010777607
IFI35	-0,39	0,039516673
BATF2	-0,39	0,041688705
PNPT1	-0,29	0,037644415
PML	-0,22	0,030117951
MAP3K9	0,34	0,010663036
FIGF	0,60	0,000923682
DUSP2	0,65	0,000736741
S100A8	0,65	7,22E-08
ALOX12B	0,66	6,43E-06
EGR1	0,66	3,18E-06
MANF	0,66	1,07E-07
CST6	0,67	5,62E-06
CPNE7	0,67	2,13E-06
POMC	0,68	0,000202198
FSCN1	0,69	4,83E-07
PPIF	0,70	7,83E-07
PGD	0,71	2,20E-05
CSK	0,73	0,016210156
MPHOSPH6	0,74	1,41E-06
FABP5	0,77	1,47E-09
CBR1	0,82	1,16E-05
CHRM1	0,85	4,90E-06
TNXB	0,86	5,07E-06
S100A9	0,86	1,09E-09
WNT5A	0,86	1,11E-08
LCN2	0,88	1,41E-06
AhRR	0,90	2,04E-05
AREG	0,93	4,67E-07
IFI30	1,00	4,21E-11
HMOX1	1,05	1,50E-11
MMP1	1,05	4,94E-12
GAL	1,12	3,20E-11
IL1A	1,20	4,85E-12
SPRR1A	1,20	2,65E-13
IL36G	1,23	7,89E-11
EPHX1	1,24	0,000139207
ARG1	1,29	2,74E-13
SERPINB3	1,33	1,13E-10
EREG	1,35	5,67E-11
SERPINB4	1,46	3,19E-08
ALDH1A3	1,48	8,05E-11
TGM3	1,49	1,42E-07
SLC45A4	1,59	1,85E-11
SECTM1	1,70	1,96E-13
SPRR2C	1,98	1,08E-14
IL1B	2,50	1,11E-19
CYP1A1	4,70	4,98E-23
CYP1B1	5,56	1,51E-22

**Table 4.** Psoriasis and dermatitis differentially regulated genes. The table includes the genes involved in psoriasis and dermatitis that are differentially regulated upon stimulation with Lawsone.

a mixture of organic compounds, and their safety and carcinogenicity have not been completely elucidated<sup>56</sup>. Similarly, Henna extracts contain hundreds of different components, including phenolic compounds, terpenes, steroids and alkaloids<sup>2</sup>, but a comprehensive investigation validating the biological activities of these compounds is still missing. The effects of Henna can result from synergistic and antagonistic properties of numerous active substances. In fact, adverse events of Henna have been described, for example after ingestion and mucosal contact<sup>57</sup>, although it appears nontoxic when applied to the skin<sup>2</sup>. Henna has been used for treating radiation-induced dermatitis, as well as for anti-carcinogenic, anti-microbial and anti-inflammatory purposes, although underlying mechanisms and molecules involved remain elusive<sup>2,3,58</sup>. Given its low cell toxicity, Lawsone has clinical potential for treatment of skin disorders characterized by hyperproliferation and inflammation. Indeed, our results demonstrate that topical administration of a cream containing small amounts of Lawsone ameliorates the irritation by a chemical insult. Similarly, topical application of FICZ ointment reduces the inflammation in a mouse model of chronic mite-induced dermatitis<sup>59</sup> while intraperitoneal injection of FICZ reduces inflammation in a psoriasis-like skin model<sup>31</sup>. Current strategies to ameliorate psoriasis explore potential therapies by modulating expression of inflammatory cytokines, including IL-17<sup>60</sup>. Curiously, in an Imiquimod-induced psoriasis model in mice, we observed a consistent reduction of IL-17 expression upon Lawsone topical exposure (unpublished data), pointing to potential therapeutic applications of Lawsone in skin disorders involving IL-17. Therefore, as an alternative to treatments using an undefined mixture of compounds (e.g. coal tar or Henna), we propose the Henna pigment Lawsone, and other naturally occurring naphthoquinones, as promising therapeutic candidate medicines for skin diseases. The 1,4-naphthoquinones form a family of natural pigments isolated from plants and fungi, widely used for staining food, clothing, skin and hair and in traditional medicine<sup>61</sup>. These include Vitamin K, Shikonin from the Chinese herb *Lithospermum erythrorhizon*<sup>62</sup> and Juglone from the Black Walnut tree<sup>63</sup> that also activate AhR (unpublished data).

In conclusion, we demonstrate that the worldwide used natural product Henna and its pigment Lawsone, are sensed by AhR thereby impacting skin homeostasis. Therefore, although different AhR ligands may act as “double-edged sword” and pose harm or benefit depending on the structure and pathophysiological context, such features should be explored as future treatment options for specific dermatologic pathologies.

## Materials and Methods

**1,4-naphthoquinone compounds and AhR agonists/antagonist.** Lawsone (2-hydroxy-1,4-naphthoquinone), Dioxin (TCDD, 2,3,7,8-tetrachlorodibenzo-p-dioxin), Phthiocol (Pht, 2-hydroxy-3-methyl-1,4-naphthoquinone) were obtained from Sigma-Aldrich, and CH223191 from Santa Cruz Biotech. All compounds were solubilized in DMSO. Henna was acquired in a conventional shop and dissolved in water. To ensure that the concentration of Lawsone in the Henna preparation was comparable to that of the purified pigment employed in our experiments, we quantified the amount of Lawsone contained in the commercial Henna powder preparation by thin-layer chromatography (TLC).

**In silico homology modeling.** A BLAST search with the sequence of hAhR PASB as a template revealed 58 hits in the Protein Data Bank (PDB) of experimental crystal structures. Based on sequence alignment, similarities, as well as bound ligands, 7 crystal structures were selected for a multiple sequence alignment and used to build a multiple template-based homology model of hAhR PASB. Apart from X-ray complex of HIF2 $\alpha$ /ARNT, previously used as single template<sup>64–66</sup>, we additionally downloaded HIF2 $\alpha$  complexed with agonists and antagonists (PDB ID: 3F1O, 4GHI, 4GS9, 4H6J, 5TBM (chainA)), homologous complexes of HIF1 $\alpha$  (4ZPR (chain B)) and of Clock/BMAL1 (4F3L) from the PDB and isolated the respective chains. Modeller 9.17 was used to create the multiple template-based homology model of hAhR. The resulting models were ranked by DOPE scoring. The best scoring model was selected for all subsequent modeling activities. Subsequently, model quality was checked, and the Protein Preparation wizard included in Maestro11v0 software (Schrödinger, LLC, New York, NY, 2018) was used to adjust structural defects using default values. All ligands were downloaded from Pubchem and thereafter analyzed by the Ligand Preparation Wizard to correct improper connectivity.

**In silico docking studies.** Molecular docking was performed using Glide included in Maestro 11v0 software. Glide docking methodologies use hierarchical filters searching for possible ligand positions in the receptor binding-site region. Initially we set up the receptor grid defining the shape and properties of the receptor binding site important for scoring the ligand poses in later steps. Ligand flexibility was accounted by exhaustive sampling of ligand torsions during the docking process and suitable poses selected for further refinement of torsional space in the field of the receptor. Finally, in a post-docking minimization the selected poses were minimized with full ligand flexibility. The docking results were ranked by GlideScore.

The receptor grid for the hAhR homology models was set up using default parameters. Flexible ligand docking was carried out in a standard precision (SP) approach. The resulting GlideScore is an estimate of the binding affinity. Molecular mechanics application Prime MM-GBSA was used for rescoring the docking poses. MM-GBSA binding energies (MMGBSA  $\Delta G$  Bind) are approximate free binding energies of protein-ligand complexes, with a more negative value indicating stronger binding.

**AhR binding studies.** AhR binding experiments were performed as described previously<sup>67</sup>. Briefly, livers from WT mice were collected and minced in MDEG buffer (25 mM MOPS, 1 mM DTT, 1 mM EDTA and 10% Glycerol, pH 7.5). Lysates were further homogenized, ultracentrifuged (100,000 g, 1 h) and the cytosolic fraction collected. Protein concentration was determined and diluted to a final concentration of 5 mg of cytosol protein/mL. Binding studies were performed upon overnight 4 °C incubation with [<sup>3</sup>H] TCDD, in the presence or absence of an excess of unlabeled TCDD. After incubation, charcoal Norit A suspension was added into the reaction mixture and incubated on ice. After centrifugation (25,000 g, 15 min at 4 °C), radioactivity was measured in a scintillation counter.

**Cell culture and stimulation.** Human epidermal keratinocytes (HEK) (Life Technologies) were grown in Epilife medium containing human keratinocyte growth supplement (Life technologies) and 1% (v/v) penicillin–streptomycin–gentamycin (GIBCO). Cells were used between 50–70% of confluence to avoid spontaneous differentiation due to dense cultures and up to three passages. Cells were trypsinized 15 minutes (min) at 37 °C, washed with blocking buffer (PBS + 1% FCS) at 180 g for 7 min, counted and plated overnight. HEK cells were then incubated with Lawsone or positive controls as indicated in the text, in the absence of epidermal growth factor, and analyzed at different time points. For AhR inhibition 12 μM of the AhR inhibitor CH223191 was added to HEK cells 1 hour (h) before stimulation with the AhR activators. Alternatively, HEK cells were treated for 24 h with ON-TARGET plus siRNA AHR (NM\_001621) and ON-TARGETplus Non-targeting Pool (Table S1, Dharmacon), according to manufacturer's instructions. Cells were then stimulated with ligands, and *CYP1A1* transcripts analyzed after 4 or 24 h. *CYP1A1* expression was normalized to glyceraldehyde-3-phosphate dehydrogenase (*GAPDH*) and results shown as fold induction ( $2^{-\Delta\Delta Ct}$ ) against non-transfected cells treated with the vehicle control (DMSO).

In some experiments, cells were pretreated for 15 min with 1 μM of the AP-1 inhibitor TIIA (Sigma-Aldrich) before stimulation with AhR activators. The time was selected by measuring the inhibition of *CSF3* expression (target of AP1)<sup>36</sup>.

HaCaT cells (Human keratinocyte cell line provided by DKFZ, Heidelberg and CLS)<sup>68</sup> and THP1 cells (human monocytes, ATCC TIB-202, Wesel, Germany) were grown in DMEM and RPMI 1640, respectively. Both media were supplemented with 10% fetal calf serum (FCS), 1% (v/v) penicillin–streptomycin, 1% (v/v) gentamycin, 1% (v/v) sodium pyruvate, 1% (v/v) L-glutamine, 1% (v/v) non-essential amino acids, 1% (v/v) HEPES buffer and 0.05% M2-mercaptoethanol (all reagents provided by GIBCO). Cells were kept at 37 °C in 5% CO<sub>2</sub>. THP-1 cells were differentiated into macrophages by treatment with 200 nM of phorbol-12-myristate-13-acetate (PMA, Sigma-Aldrich).

**Lentiviral infection and reporter cell line development.** The construct for generation of the AhR reporter cell lines was obtained from SABiosciences ([http://www.sabiosciences.com/reporter\\_assay\\_product/HTML/CLS-9045L.html](http://www.sabiosciences.com/reporter_assay_product/HTML/CLS-9045L.html)). Briefly, the Cignal™ Lenti XRE Reporter is a replication incompetent, VSV-g pseudotype lentivirus expressing the firefly luciferase gene under the control of a minimal (m) CMV promoter and tandem repeats of the dioxin-responsive element (DRE). Upon stimulation of the AhR pathway, induction of luciferase expression can be used as readout of activation. Lentiviral infection was performed according to the protocols available at RNAi Consortium website ([https://www.broadinstitute.org/genome\\_bio/trc/publicProtocols.html](https://www.broadinstitute.org/genome_bio/trc/publicProtocols.html)).  $2.2 \times 10^4$  cells per well in a 96 well plate (NUNC) were plated overnight. Following day, medium was removed and lentiviruses were added to the cells in medium containing 8 mg/ml of polybrene (Sigma-Aldrich). Plates were spun down for 90 min at 2200 rpm at 37 °C. Transduced cells were further selected using puromycin (Calbiochem; 5 mg/ml) 2 days (d) after infection.

**Luciferase assay.** AhR reporter cell lines were stimulated for specified time and concentration of the ligand. Cells were harvested in reporter lysis buffer (Promega) and supernatant used to determine luciferase activity using Dual-Glo Luciferase Assay System (Promega) according to manufacturer's instructions. Luciferase activity was normalized to the amount of protein determined by Bradford reaction (Protein Assay Kit, Pierce). Results are shown as fold induction by normalizing the activation of the different compounds against non-stimulated or vehicle control.

**Ex vivo stimulation of skin biopsies.** Skin was cut in small pieces (1 cm<sup>2</sup>) and treated 24 h with vehicle control (DMSO) or 10 μM of Lawsone followed by cell disruption and lysis in Trizol.

**Stimulation and development of human epidermal skin equivalents.** Undifferentiated human epidermal skin equivalents (EpiDerm model, EPI-201, MatTek Corporation) were cultured at the air–liquid interface for 10d. Cells were daily treated with 10 μM or 100 μM of Lawsone or DMSO.

**Immunostaining of HEK cells or human skin equivalents and image analysis.** Cytotoxicity of Lawsone was measured by phosphorylation at Ser139 residues of the H2A.X histone. Phosphorylation of the H2A.X histone occurs at the site of DNA damage after exposure to polyaromatic hydrocarbons, hydroxyl radicals or ionizing radiation<sup>69</sup>. 4 h after Lawsone exposure, HEK cells were fixed with 2% paraformaldehyde for 20 min at room temperature (RT) and permeabilized with 0.1% Triton for 5 min at RT. After 30 minutes in blocking buffer, cells were stained with α-phospho-Histone H2A.X (Millipore) for 1 h at RT, followed by staining with the α-rabbit IgG AlexaFluor488 (Dianova,) for 1 h at RT. Nuclei were stained using Nuc red Live 647 (Life technologies). Cell image acquisition and analysis was performed using Arrayscan XTI Live High Content Platform (ThermoFisher Scientific).

Formalin-fixed paraffin-embedded skin equivalents were stained either with hematoxylin and eosin (Sigma-Aldrich) or anti-human cornifelin (Sigma) and loricrin (Abcam), followed by anti-rabbit AlexaFluor555 and 488 respectively. Nuclei were counterstained with DAPI. Images were acquired using a Leica DMRB fluorescent microscope and analyzed with ImageJ (<https://imagej.nih.gov/ij/>).

**RT-PCR and RT-PCR multiplex gene expression profiling.** Total RNA was extracted using 500 μL of trizol (Life technologies), followed by chloroform (1:5) and isopropanol (1:2) phase separation. RNA was washed with ethanol and resuspended in RNase free water. RNA quality and concentration were determined by spectrophotometry (Nanodrop 2000c, ThermoFisher Scientific). Complementary DNA (cDNA) synthesis was generated using Superscript III Reverse Transcriptase (Invitrogen), according to manufacturer's instructions.



Quantitative RT–PCR was performed using TaqMan master mix (Life technologies). In some experiments multiplex gene expression profiling was performed using the Biomark HD of Fluidigm as previously described<sup>70</sup>. Gene expression was normalized to *GAPDH*. The average threshold cycle of triplicate reactions was employed for all subsequent calculations as  $2^{-\delta\Delta Ct}$  relative to vehicle control (DMSO). Taqman probes (Life technologies) are listed in Table S1.

**Western blotting analysis.** Proteins of human skin equivalents were isolated with radioimmunoprecipitation assay buffer and protein concentrations analyzed with the Pierce BCA Protein Assay Kit (Thermo Fisher Scientific), according to the manufacturer's instructions. Anti-human cornifelin and flaggrin were purchased from Sigma and anti-human loricrin from Abcam.

AhR protein in HEK was detected after cell lysis with RIPA buffer. Protein amount was quantified using Pierce BCA Protein Assay Kit (Thermo Fisher Scientific), according to the manufacturer's instructions. 30 µg protein were diluted in Laemmli buffer containing β-mercaptoethanol and loaded on a Mini Protean TGX Stain Free precast Gel. AhR protein was detected by ECL, using anti-AhR polyclonal antibody. (Enzo Life sciences) and β-Actin expression (Abcam) was used as a loading control.

**Lactate dehydrogenase (LDH) assay.** LDH was purchased from Pierce™ (Thermo Scientific) and used according to the manufacturer's instruction. Percentage (%) of cytotoxicity was calculated as:

$$\frac{(\text{compound treated LDH activity} - \text{spontaneous LDH activity}) \times 100}{(\text{maximum LDH activity} - \text{spontaneous LDH activity})}$$

**Ethoxyresorufin-O-deethylase (EROD) activity.** The enzymatic activity of CYP1A1 was used as readout of AhR activation. The EROD assay detects the CYP1A1 enzymatic activity by measuring the conversion of ethoxyresorufin into resorufin<sup>71</sup> in the medium of HEK cells. Briefly after 48 h of stimulation with AhR activators, 4 µM resorufin ethyl ether (EROD, Sigma-Aldrich) and 10 µM dicoumarol (Sigma-Aldrich) were added to HEK culture for 1 h and activity measured with the Fluoroskan Ascent Microplate Fluorometer (Thermo LabSystem). The activity was corrected to the amount of protein measured by Bradford assay and normalized to the vehicle control (DMSO).

**In vivo zebrafish experiments.** Fertilized embryos were used for all experiments. One day post fertilization (dpf) larvae were manually dechorionated under a Leica MZ6 Stereomicroscope. Each experimental group consisted of 12 larvae unless stated otherwise.

**Larval exposure experiments.** In larval exposure experiments, 2dpf AB strain larvae were exposed to different ligands for 4 h, in the presence or absence of CH223191 (5 µM). After exposure, larvae were euthanized with Tricaine (MS-222, 300 µg/mL SIGMA)<sup>72</sup> and placed in Trizol for RNA isolation or used for EROD experiments performed as described previously<sup>73</sup>. Briefly, After exposure, zebrafish larvae were washed and placed in medium containing 0.4 µg/mL of 7-ethoxyresorufin (Cayman Chemical) for 5 min. Non-fluorescent 7-ethoxyresorufin diffuses into the embryo and is O-deethylated into resorufin, a fluorescent product that can be measured<sup>73</sup>. Embryos were anesthetized with Tricaine (MS-222 168 µg/mL, SIGMA)<sup>74</sup>, placed in black 96 well plates with clear bottom (Thermo Fisher) and imaged in an Array Scan™ XTI Live High Content Platform (Thermo Fisher). Brightfield images were used to identify shape of fish and fluorescence (filters excitation: 549/15 nm, emission: 590–624 nm) was determined per fish as a readout of CYP1A activation. Syber-green primers (Eurofins) are listed in Table S1.

**Larval tail fin regeneration.** 2dpf AB larvae were anesthetized with Tricaine (MS-222, 200 µg/mL, Sigma) and tail fin was amputated as described previously<sup>41</sup>. After amputation, larvae were exposed to different ligands for 1 h. After exposure and several washes with embryo medium, larvae were kept for 3d in an incubator at 28°C with cycles of 14 h of light and 10 h of darkness. Afterwards, larvae were anesthetized with Tricaine (MS-222, 168 µg/mL, Sigma) and visualized in an M205 Leica stereomicroscope. Data analysis was performed on ImageJ software (<https://imagej.nih.gov/ij/>).

**Zebrafish cell migration.** The transgenic line used in the study was mpeg.mCherryCAAX SH378 mpx:GFP i114, where neutrophils stably express GFP<sup>44,45</sup>. Imaging was performed on 3dpf larvae treated, wounded and mounted as reported previously<sup>75</sup>. Briefly, embryos were pretreated with 10 µM Lawsone or DMSO, in E3-tricaine solution (E3/T; Sigma; 200 µg/mL) for 1 h. Fish were anaesthetized in Lawsone-containing E3/T, and a section of the tail was cut using a razor blade. Fish were then embedded lateral side down in 1% low melting point agarose (dissolved in E3/T), over MatTek glass bottom culture dishes and overlaid with the drug in E3/T. Time-lapse fluorescence images were acquired with an Andor Revolution spinning-disk confocal unit equipped with an inverted Nikon Eclipse Ti microscope and an XYZ motorized stage, coupled to an EMCCD camera (Andor) and a Yokogawa CSU-X1 scanning head and driven by Andor iQ 2.5.1 software. GFP imaging was performed using 488-nm laser line.

Image sequences were generated every minute using a 20X NA 0.75/20X Super Fluor objective and 3.44 µm step size. Bright field images were taken at low-level illumination with a halogen lamp. Where indicated, images were processed with Manual Tracking module (ImageJ software, NIH) on maximum intensity projection. Upon background subtraction for each fluorescence channel, a Gaussian blur filter was applied. Brightness and contrast were set and then multi-channel image sequences were overlaid.

**Zebrafish cell dynamics analysis.** Neutrophils were tracked with the Manual Tracking plugin (ImageJ). The resulting 2D coordinates were analyzed using the Chemotaxis Tool plugin (Ibidi, Germany).

([http://ibidi.com/fileadmin/products/software/chemotaxis\\_tool/IN\\_XXXXX\\_CT\\_Tool\\_2\\_0.pdf](http://ibidi.com/fileadmin/products/software/chemotaxis_tool/IN_XXXXX_CT_Tool_2_0.pdf)).

Directionality of the path represents a measurement of the straightness of cell trajectories and is calculated as:

$$D = \frac{d_{euclid}}{d_{accum}}$$

where  $d_{accum}$  is the accumulated distance of the cell path and the  $d_{euclid}$  is the length of the straight line between cell start and end point<sup>76</sup>.

The forward migration index represents the efficiency of the forward migration of cells towards the wound, and is calculated as:

$$FMI^{wound} = \frac{x_{end}}{d_{accum}}$$

where  $x_{end}$  is the cell end position in the axis towards the wound.

**Mouse wound healing experiments.** C57BL/6 mice were bred and housed in community cages at the Animal Care Facilities of the MPIIB, Marienfelde, Berlin. Mice were used at 7–8 weeks of age. An excision of 6 mm was performed at the back of the mice anesthetized with Isofluran. The wound was immediately treated with Lawsone (10  $\mu$ M) or DMSO in PBS. Treatment was followed up for 5 consecutive days. Pictures were taken daily until day 6 using a Fujifilm FinePix S5800 camera. Analysis of the data was performed using ImageJ software (<https://imagej.nih.gov/ij/>). To calculate the size of the wounds the circumference was normalized to the length of an internal control (1 cm of the ruler in the picture) and results were further normalized to day 0.

**Contact skin irritation model.** Skin irritation was induced with 5% sodium dodecyl sulfate (SDS) in conserved water DAC (NRF S.6) on 4 spots of the volar forearm of 9 subjects using round self-adhesive patches with a diameter of 1.2 cm (Curatest<sup>®</sup>F, Lohmann & Rauscher, Germany). Patches were removed after 24 h and the skin was carefully cleaned with water. Lawsone was applied to the SDS treated sites at concentrations of 0.5%, 1% and 3% (g/g) in base cream. Pure base cream served as an intra-individual control. Treatment sites were covered by self-adhesive patches for another 24 h. The extent of skin irritation was assessed by using Moor Full-field Laser Perfusion Imager (FLPI-2, Moor Instruments, Axminster, UK) at time points 2, 3 and 7 days after induction of skin irritation.

**Microarray hybridization protocol, data preprocessing and analysis.** Gene expression microarray studies were carried out as dual-color hybridization of HEK cells from one donor. RNA labeling was performed with the Quick Amp Labeling Kit, two-color (Agilent Technologies). In brief, mRNA was reverse transcribed and amplified using an oligo-dT-T7 promoter primer, T7 RNA Polymerase and Cyanine 3-CTP or Cyanine 5-CTP. After precipitation, purification, and quantification, 300 ng cRNA of both samples were pooled, fragmented and hybridized to custom-commercial whole genome human 8  $\times$  60 k multipack microarrays (Agilent-048908) according to the supplier's protocol (Agilent Technologies). Scanning of microarrays was performed with 3  $\mu$ m resolution using a G2565CA high-resolution laser microarray scanner (Agilent Technologies). Microarray image data were processed with the Image Analysis/Feature Extraction software G2567AA v. A.11.5.1.1 (Agilent Technologies) using default settings and the GE2\_1105\_Oct12 extraction protocol.

The extracted single-color raw data txt files were analyzed using R and the associated BioConductor *limma* R package<sup>77,78</sup> for differential expression analysis. The data set was background corrected and normalized using *loess* method. Microarray data were deposited in the NCBI's Gene Expression Omnibus (GEO, accession number GSE99901).

We used the *lmFit* function to fit a linear model which included the factors stimulus type (Lawsone and Pam2CSK4) and treatment (stimulated/control) as well as an interaction term. The p-values were calculated based on moderated t statistics and most differentially regulated genes were retrieved with *topTable* function from *limma* package.

Genes associated with AhR and Nrf2 activation or keratinocyte differentiation were manually chosen on the basis of literature, and three custom gene lists were created: AhR dependent-genes (Table 1), Nrf2-related genes (Table 2) and EDC-keratin genes (Table 3). Gene set enrichment analysis was performed and visualized using R-package *tmod* for analysis of transcriptional modules<sup>79</sup>. In the first step, CERNO statistical test was applied to the list of genes contained in the linear fit model with *tmodLimmaTest* function. Next, a ROC curve was plotted for the respective modules using *evidencePlot* function from *tmod* package<sup>29,78</sup>. Genes presenting highest influence on the module enrichment were identified and labeled on the ROC curve. Statistical script in R including all steps of the microarray analysis can be obtained by request.

Ingenuity Pathway Analysis (<https://www.qiagenbioinformatics.com/products/ingenuity-pathway-analysis/>, version 33559992) was performed to identify the top canonical pathways differentially regulated upon 4 h stimulation of HEK cells with Lawsone (10  $\mu$ M) as compared to DMSO. Pathway analysis was performed using log2 fold changes and p-values obtained from comparisons between the different stimuli.

**Statistical analysis.** Statistical analysis was performed with GraphPad Prism v7.03 (GraphPad software Inc., USA). P-values were calculated using student's t-test, One-Way or Two-Way ANOVA as stated for each experiment. The confidence interval used is 95%. P-value (P) \* < 0.05; \*\* < 0.01; \*\*\* < 0.001; \*\*\*\* < 0.0001.

**Study approval.** All methods were carried out in accordance with relevant guidelines and regulations. All experimental protocols were approved by the respective licensing committees. Skin biopsies were obtained from healthy human volunteers under ethical approval of the Committee of Ethics and Academic and Scientific Deontology, Ministry of Education and Scientific Research, University of Medicine and Pharmacy of Craiova, Romania (Number 117/27.05.2015). Skin irritation experiments were performed in accordance with the guidelines set out by the State Agency for Health and Social Affairs (LaGeSo, Berlin, Germany), project number EA1/1855/17. Informed consent was obtained from all the subjects participating to the study.

Mouse experiments were performed in accordance with guidelines set out by LaGeSo, project number Reg 0222/16.

Zebrafish and embryos were raised and maintained according to standard protocols<sup>72</sup>. Experiments at the MPIIB were approved by, and conducted in accordance with, the guidelines set out by the LaGeSo. The Vivarium at NMS|FCM-UNL is licensed for animal work by DGAV, complying with the European Directive 2010/63/EU and the Portuguese Decree Law Number 113/2013, following the FELASA guidelines and recommendations concerning laboratory animal welfare.

## Data Availability

All data generated or analyzed during this study are included in this published article (and its Supplementary Information files). If additional details are desired, they are available from the corresponding author on request.

## References

- Krutmann, J., Bouloc, A., Sore, G., Bernard, B. A. & Passeron, T. The skin aging exposome. *J Dermatol Sci* **85**, 152–161 (2017).
- Badoni, S. R., Semwal, D. K., Combrinck, S., Cartwright-Jones, C. & Viljoen, A. Lawsonia inermis L. (henna): ethnobotanical, phytochemical and pharmacological aspects. *J Ethnopharmacol* **155**, 80–103 (2014).
- Pradhan, R. *et al.* From body art to anticancer activities: perspectives on medicinal properties of henna. *Curr Drug Targets* **13**, 1777–1798 (2012).
- Ip, N. & Hoddes, J. Henna tattoo: infection or allergy? *Lancet* **383**, 1436 (2014).
- Goldenberg, A. & Jacob, S. E. Paraphenylenediamine in black henna temporary tattoos: 12-year Food and Drug Administration data on incidence, symptoms, and outcomes. *J Am Acad Dermatol* **72**, 724–726 (2015).
- de Groot, A. C. Side-effects of henna and semi-permanent 'black henna' tattoos: a full review. *Contact Dermatitis* **69**, 1–25 (2013).
- Kraeling, M. E., Bronaugh, R. L. & Jung, C. T. Absorption of lawsone through human skin. *Cutan. Ocul. Toxicol* **26**, 45–56 (2007).
- Moura-Alves, P. *et al.* AhR sensing of bacterial pigments regulates antibacterial defence. *Nature* **512**, 387–392 (2014).
- Esser, C., Barga, I., Weighardt, H., Haarmann-Stemmann, T. & Krutmann, J. Functions of the aryl hydrocarbon receptor in the skin. *Semin. Immunopathol* **35**, 677–691 (2013).
- Hahn, M. E., Karchner, S. I., Shapiro, M. A. & Perera, S. A. Molecular evolution of two vertebrate aryl hydrocarbon (dioxin) receptors (AHR1 and AHR2) and the PAS family. *Proc. Natl. Acad. Sci. USA* **94**, 13743–13748 (1997).
- Stockinger, B., Di, M. P., Gialitakis, M. & Duarte, J. H. The aryl hydrocarbon receptor: multitasking in the immune system. *Annu. Rev Immunol* **32**, 403–432 (2014).
- Mandal, P. K. Dioxin: a review of its environmental effects and its aryl hydrocarbon receptor biology. *J Comp Physiol B* **175**, 221–230 (2005).
- Miniero, R., De, F. E., Ferri, F. & di, D. A. An overview of TCDD half-life in mammals and its correlation to body weight. *Chemosphere* **43**, 839–844 (2001).
- Murray, I. A., Patterson, A. D. & Perdew, G. H. Aryl hydrocarbon receptor ligands in cancer: friend and foe. *Nat Rev Cancer* **14**, 801–814 (2014).
- Fritsche, E. *et al.* Lightening up the UV response by identification of the arylhydrocarbon receptor as a cytoplasmic target for ultraviolet B radiation. *Proc. Natl. Acad. Sci. USA* **104**, 8851–8856 (2007).
- Opitz, C. A. *et al.* An endogenous tumour-promoting ligand of the human aryl hydrocarbon receptor. *Nature* **478**, 197–203 (2011).
- Nguyen, L. P. & Bradfield, C. A. The search for endogenous activators of the aryl hydrocarbon receptor. *Chem Res Toxicol* **21**, 102–116 (2008).
- Li, Y. *et al.* Exogenous stimuli maintain intraepithelial lymphocytes via aryl hydrocarbon receptor activation. *Cell* **147**, 629–640 (2011).
- Schiering, C. *et al.* Feedback control of AHR signalling regulates intestinal immunity. *Nature* **542**, 242–245 (2017).
- Esser, C. & Rannug, A. The aryl hydrocarbon receptor in barrier organ physiology, immunology, and toxicology. *Pharmacol Rev* **67**, 259–279 (2015).
- Mulero-Navarro, S. & Fernandez-Salguero, P. M. New Trends in Aryl Hydrocarbon Receptor Biology. *Front Cell Dev Biol* **4**, 45 (2016).
- van den Bogaard, E. H. *et al.* Genetic and pharmacological analysis identifies a physiological role for the AHR in epidermal differentiation. *J Invest Dermatol* **135**, 1320–1328 (2015).
- Eckert, R. L. & Rorke, E. A. Molecular biology of keratinocyte differentiation. *Environ Health Perspect* **80**, 109–116 (1989).
- Poland, A., Glover, E. & Kende, A. S. Stereospecific, high affinity binding of 2,3,7,8-tetrachlorodibenzo-p-dioxin by hepatic cytosol. Evidence that the binding species is receptor for induction of aryl hydrocarbon hydroxylase. *J Biol Chem* **251**, 4936–4946 (1976).
- Haarmann-Stemmann, T., Esser, C. & Krutmann, J. The Janus-Faced Role of Aryl Hydrocarbon Receptor Signaling in the Skin: Consequences for Prevention and Treatment of Skin Disorders. *J Invest Dermatol* **135**, 2572–2576 (2015).
- Kim, S. H. *et al.* Novel compound 2-methyl-2H-pyrazole-3-carboxylic acid (2-methyl-4-o-tolylazo-phenyl)-amide (CH-223191) prevents 2,3,7,8-TCDD-induced toxicity by antagonizing the aryl hydrocarbon receptor. *Mol. Pharmacol* **69**, 1871–1878 (2006).
- Wincent, E. *et al.* Biological effects of 6-formylindolo[3,2-b]carbazole (FICZ) *in vivo* are enhanced by loss of CYP1A function in an Ahr2-dependent manner. *Biochem Pharmacol* **110–111**, 117–129 (2016).
- Schiwy, A. *et al.* Determination of the CYP1A-inducing potential of single substances, mixtures and extracts of samples in the micro-EROD assay with H4IIE cells. *Nat Protoc* **10**, 1728–1741 (2015).
- Weiner, J. III. & Domaszewska, T. tmod: an R package for general and multivariate enrichment analysis. *PeerJ Preprints* **e2420v1** (2016).
- Baird, L. & Dinkova-Kostova, A. T. The cytoprotective role of the Keap1-Nrf2 pathway. *Arch. Toxicol* **85**, 241–272 (2011).
- Di Meglio, P. *et al.* Activation of the aryl hydrocarbon receptor dampens the severity of inflammatory skin conditions. *Immunity* **40**, 989–1001 (2014).
- Haas, K. *et al.* Aryl Hydrocarbon Receptor in Keratinocytes Is Essential for Murine Skin Barrier Integrity. *J Invest Dermatol* **136**, 2260–2269 (2016).
- Sutter, C. H., Bodreddigari, S., Campion, C., Wible, R. S. & Sutter, T. R. 2,3,7,8-Tetrachlorodibenzo-p-dioxin increases the expression of genes in the human epidermal differentiation complex and accelerates epidermal barrier formation. *Toxicol Sci* **124**, 128–137 (2011).

34. van den Bogaard, E. H. *et al.* Coal tar induces AHR-dependent skin barrier repair in atopic dermatitis. *J Clin. Invest* **123**, 917–927 (2013).
35. Eckert, R. L. *et al.* AP1 transcription factors in epidermal differentiation and skin cancer. *J Skin Cancer* **2013**, 537028 (2013).
36. Tseng, H. C. *et al.* IL-1beta promotes corneal epithelial cell migration by increasing MMP-9 expression through NF-kappaB- and AP-1-dependent pathways. *PLoS. One* **8**, e57955 (2013).
37. King-Heiden, T. C. *et al.* Reproductive and developmental toxicity of dioxin in fish. *Mol Cell Endocrinol* **354**, 121–138 (2012).
38. Rakers, S. *et al.* 'Fish matters': the relevance of fish skin biology to investigative dermatology. *Exp Dermatol* **19**, 313–324 (2010).
39. Jonsson, M. E., Jenny, M. J., Woodin, B. R., Hahn, M. E. & Stegeman, J. J. Role of AHR2 in the expression of novel cytochrome P450 1 family genes, cell cycle genes, and morphological defects in developing zebra fish exposed to 3,3',4,4',5-pentachlorobiphenyl or 2,3,7,8-tetrachlorodibenzo-p-dioxin. *Toxicol Sci* **100**, 180–193 (2007).
40. Li, Q., Frank, M., Thisse, C. I., Thisse, B. V. & Uitto, J. Zebrafish: a model system to study heritable skin diseases. *J Invest Dermatol* **131**, 565–571 (2011).
41. Mathew, L. K., Andreasen, E. A. & Tanguay, R. L. Aryl hydrocarbon receptor activation inhibits regenerative growth. *Mol Pharmacol* **69**, 257–265 (2006).
42. Zodrow, J. M. & Tanguay, R. L. 2,3,7,8-tetrachlorodibenzo-p-dioxin inhibits zebrafish caudal fin regeneration. *Toxicol Sci* **76**, 151–161 (2003).
43. Cordeiro, J. V. & Jacinto, A. The role of transcription-independent damage signals in the initiation of epithelial wound healing. *Nat Rev Mol Cell Biol* **14**, 249–262 (2013).
44. Bojarczuk, A. *et al.* Cryptococcus neoformans Intracellular Proliferation and Capsule Size Determines Early Macrophage Control of Infection. *Sci Rep* **6**, 21489 (2016).
45. Renshaw, S. A. *et al.* A transgenic zebrafish model of neutrophilic inflammation. *Blood* **108**, 3976–3978 (2006).
46. Grose, R. & Werner, S. Wound-healing studies in transgenic and knockout mice. *Mol Biotechnol* **28**, 147–166 (2004).
47. Lammintausta, K., Maibach, H. I. & Wilson, D. Susceptibility to cumulative and acute irritant dermatitis. An experimental approach in human volunteers. *Contact Dermatitis* **19**, 84–90 (1988).
48. Geusau, A. *et al.* 2,3,7,8-tetrachlorodibenzo-p-dioxin impairs differentiation of normal human epidermal keratinocytes in a skin equivalent model. *J Invest Dermatol* **124**, 275–277 (2005).
49. Osborne, R. & Greenlee, W. F. 2,3,7,8-Tetrachlorodibenzo-p-dioxin (TCDD) enhances terminal differentiation of cultured human epidermal cells. *Toxicol Appl. Pharmacol* **77**, 434–443 (1985).
50. Bergander, L. *et al.* Metabolic fate of the Ah receptor ligand 6-formylindolo[3,2-b]carbazole. *Chem. Biol. Interact* **149**, 151–164 (2004).
51. Caputo, R. *et al.* Cutaneous manifestations of tetrachlorodibenzo-p-dioxin in children and adolescents. Follow-up 10 years after the Seveso, Italy, accident. *J Am. Acad. Dermatol* **19**, 812–819 (1988).
52. Ju, Q., Zouboulis, C. C. & Xia, L. Environmental pollution and acne: Chloracne. *Dermatoendocrinol* **1**, 125–128 (2009).
53. Tauchi, M. *et al.* Constitutive expression of aryl hydrocarbon receptor in keratinocytes causes inflammatory skin lesions. *Mol Cell Biol* **25**, 9360–9368 (2005).
54. Yeager, R. L., Reisman, S. A., Aleksunes, L. M. & Klaassen, C. D. Introducing the "TCDD-inducible AhR-Nrf2 gene battery". *Toxicol Sci* **111**, 238–246 (2009).
55. Tsuji, G. *et al.* Identification of ketoconazole as an AhR-Nrf2 activator in cultured human keratinocytes: the basis of its anti-inflammatory effect. *J Invest Dermatol* **132**, 59–68 (2012).
56. Van Ruissen, F. *et al.* Induction of normal and psoriatic phenotypes in submerged keratinocyte cultures. *J Cell Physiol* **168**, 442–452 (1996).
57. Kok, A. N., Ertekin, V., Bilge, Y. & Isik, A. F. An unusual cause of suicide: henna (*Lawsonia inermis* Linn.). *J Emerg Med* **29**, 343–344 (2005).
58. Ansari, M. *et al.* Efficacy of topical alpha ointment (containing natural henna) compared to topical hydrocortisone (1%) in the healing of radiation-induced dermatitis in patients with breast cancer: a randomized controlled clinical trial. *Iran J Med. Sci* **38**, 293–300 (2013).
59. Kiyomatsu-Oda, M., Uchi, H., Morino-Koga, S. & Furue, M. Protective role of 6-formylindolo[3,2-b]carbazole (FICZ), an endogenous ligand for arylhydrocarbon receptor, in chronic mite-induced dermatitis. *J Dermatol Sci* **90**, 284–294 (2018).
60. Lowes, M. A., Russell, C. B., Martin, D. A., Towne, J. E. & Krueger, J. G. The IL-23/T17 pathogenic axis in psoriasis is amplified by keratinocyte responses. *Trends Immunol* **34**, 174–181 (2013).
61. Grolig, J. & Wagner, R. In *Ullmann's Encyclopedia of Industrial Chemistry* Vol. 23 733 (2000).
62. Huang, C. S., Chen, H. W., Lin, T. Y., Lin, A. H. & Lii, C. K. Shikonin upregulates the expression of drug-metabolizing enzymes and drug transporters in primary rat hepatocytes. *J Ethnopharmacol* **216**, 18–25 (2018).
63. Seigler, D. S. *Plant Secondary Metabolism*. 76–93 (Springer US, 1998).
64. Bessede, A. *et al.* Aryl hydrocarbon receptor control of a disease tolerance defence pathway. *Nature* **511**, 184–190 (2014).
65. Perkins, A. *et al.* A Structural Switch between Agonist and Antagonist Bound Conformations for a Ligand-Optimized Model of the Human Aryl Hydrocarbon Receptor Ligand Binding Domain. *Biology (Basel)* **3**, (645–669 (2014).
66. Tkachenko, A. *et al.* Nuclear transport of the human aryl hydrocarbon receptor and subsequent gene induction relies on its residue histidine 291. *Arch Toxicol* (2017).
67. Montaldo, E. *et al.* Human RORgammat(+)CD34(+) cells are lineage-specified progenitors of group 3 RORgammat(+) innate lymphoid cells. *Immunity* **41**, 988–1000 (2014).
68. Boukamp, P. *et al.* Normal keratinization in a spontaneously immortalized aneuploid human keratinocyte cell line. *J Cell Biol* **106**, 761–771 (1988).
69. Muslimovic, A., Johansson, P. & Hammarsten, O. In *Current Topics in Ionizing Radiation Research* (ed M. Neno) Ch. 1 (2012).
70. Lozza, L. *et al.* Crosstalk between human DC subsets promotes antibacterial activity and CD8+ T-cell stimulation in response to bacille Calmette-Guerin. *Eur. J Immunol* **44**, 80–92 (2014).
71. Mohammadi-Bardbori, A. Assay for quantitative determination of CYP1A1 enzyme activity using 7-Ethoxyresorufin as standard substrate (EROD assay). Protocol Exchange. <https://doi.org/10.1038/protex.2014.043> (2014).
72. Nüsslein-Volhard, C. & Dahm, R. *Zebrafish: a practical approach*. (Oxford University Press 2002).
73. Nacci, D. *et al.* Nondestructive indicator of ethoxyresorufin-O-deethylase activity in embryonic fish. *Environmental Toxicology and Chemistry* **17**, 2481–2486 (1998).
74. Westerfield, M. *The Zebrafish Book. A Guide for the Laboratory Use of Zebrafish (Danio rerio)*. 5th edn, (University of Oregon Press, 2007).
75. Crespo, C. L. *et al.* The PAR complex controls the spatiotemporal dynamics of F-actin and the MTOC in directionally migrating leukocytes. *J Cell Sci* **127**, 4381–4395 (2014).
76. Petrie, R. J., Doyle, A. D. & Yamada, K. M. Random versus directionally persistent cell migration. *Nat Rev Mol Cell Biol* **10**, 538–549 (2009).
77. Ritchie, M. E. *et al.* limma powers differential expression analyses for RNA-sequencing and microarray studies. *Nucleic Acids Res* **43**, e47 (2015).
78. 3rd, J. W. R. *A language and environment for statistical computing*. R Foundation for Statistical Computing, Vienna, Austria.
79. Weiner, J. *Functional Multivariate analysis with the tmod package* (2015).

## Acknowledgements

The authors thank Mary Louise Grossman and Souraya Sibaei for excellent editorial assistance, and Philippe Saikali for technical help (Department of Immunology, Max Planck Institute for Infection Biology, Charitéplatz 1, D-10117 Berlin, Germany). We also thank Sabrina Hadam, Eva Katharina Barbosa Pfannes and Annika Vogt for fruitful discussions (Department of Dermatology and Allergy, Clinical Research Center for Hair and Skin Science, Charité-Universitätsmedizin Berlin, Germany). We acknowledge Anne Diehl (Leibniz-Forschungsinstitut fuer Molekulare Pharmakologie, Berlin, Germany) for mouse liver protein preparation. The zebrafish mpeg.mCherryCAAX SH378 mp:GFP i114 line was kindly provided by Dr. Stephen Renshaw, The University of Sheffield, UK (<http://www.sheffield.ac.uk/iicd/profiles/renshaw>).

## Author Contributions

L.L. and P.M.A. designed the study and performed the majority of experiments; T.D., J.W., H.J.M. and M.B. performed microarray analyses; A.K. and G.K. performed *in silico* analysis. J.F. performed binding studies. C.C. and A.J. performed and analyzed zebrafish wound healing experiments; I.S., S.B.U. and I.M. performed human skin biopsies experiments; A.P., R.H., M.K., U.G.B., U.Z., A.B.K. and M.S. performed experiments; M.L.M. supervised mouse experiments; F.S. and M.M. supervised the mouse wound healing experiments and performed contact skin irritation experiments; S.H.E.K. proposed and supervised project; L.L., P.M.A. analyzed data and wrote manuscript with major input from S.H.E.K.

## Additional Information

**Supplementary information** accompanies this paper at <https://doi.org/10.1038/s41598-019-47350-x>.

**Competing Interests:** The authors declare no competing interests.

**Publisher's note:** Springer Nature remains neutral with regard to jurisdictional claims in published maps and institutional affiliations.



**Open Access** This article is licensed under a Creative Commons Attribution 4.0 International License, which permits use, sharing, adaptation, distribution and reproduction in any medium or format, as long as you give appropriate credit to the original author(s) and the source, provide a link to the Creative Commons license, and indicate if changes were made. The images or other third party material in this article are included in the article's Creative Commons license, unless indicated otherwise in a credit line to the material. If material is not included in the article's Creative Commons license and your intended use is not permitted by statutory regulation or exceeds the permitted use, you will need to obtain permission directly from the copyright holder. To view a copy of this license, visit <http://creativecommons.org/licenses/by/4.0/>.

© The Author(s) 2019